Organic & Biomolecular Chemistry

7 Hz), 3.52 (1H, dq J = 14 Hz, 7 Hz), 3.95, 4.10 (2H, AB, J = 11.5 Hz), 4.07 (1H, s), 4.13 (1H, s), 4.52, 4.54 (2H, AB, J = 12 Hz), 4.59, 4.63 (2H, AB, J = 11.5 Hz), 4.70 (2H, s), 5.39 (1H, s), 5.45, 5.47 (2H, AB, J = 9.5 Hz), 7.18–7.39 (15H, m), 7.54 (1H, s). ^{13}C NMR (100 MHz, CDCl$_3$) δ: 12.8, 13.7, 36.5, 62.4, 63.2, 70.1, 72.2, 72.3, 73.7, 76.7, 78.1, 85.4, 87.6, 109.8, 127.6, 127.6, 127.9, 128.1, 128.4, 133.8, 136.3, 137.4, 137.6, 150.5, 163.1, 170.1. MS (FAB): m/z 612 [M + H]$^+$. HRMS (FAB): calcd for C$_{35}$H$_{38}$N$_3$O$_7$ [M + H]$^+$: 612.2710. Found: 612.2693.

(2'R)-3',5'-Di-O-benzyl-N^3-benzyloxymethyl-2'-propylamino-2'-N,4'-C-oxomethylenethymidine (2d: R = nPr). By following the general procedure 1, using 1-bromopropane as an alkyl halide, 2d was obtained in 76% as a white amorphous solid.

[α]$_D^{23}$ +29.2 (c 1.000, CHCl$_3$). IR (KBr): 3066, 3029, 2910, 2863, 1724, 1709, 1664, 1455, 1274 cm^{-1}. ^{1}H NMR (300 MHz, CDCl$_3$) δ: 0.93 (3H, q, J = 7.0 Hz), 1.56–1.64 (2H, m), 1.64 (3H, s), 3.33 (2H, ddq), 3.95, 4.09 (2H, AB, J = 12 Hz), 4.07 (1H, s), 4.13 (1H, s), 4.53 (2H, s), 4.59, 4.65 (2H, AB, J = 11.0 Hz), 4.71 (2H, s), 5.40 (1H, s), 5.46 (2H, t, J = 9.5 Hz), 7.19–7.37 (15H, m), 7.54 (1H, s). ^{13}C NMR (100 MHz, CDCl$_3$) δ: 11.1, 12.9, 21.9, 43.4, 62.9, 63.3, 70.2, 72.3, 72.3, 72.4, 73.8, 78.2, 85.3, 87.5, 109.8, 127.6, 127.6, 127.6, 127.7, 128.0, 128.2, 128.2, 128.2, 128.4, 133.8, 136.3, 137.4, 137.4, 137.7, 150.6, 163.2, 170.5. MS (FAB): m/z 626 [M + H]$^+$. HRMS (FAB): calcd for C$_{36}$H$_{40}$N$_3$O$_7$ [M + H]$^+$: 626.2866. Found: 626.2867.

(2'R)-3',5'-Di-O-benzyl-N^3-benzyloxymethyl-2'-isopropylamino-2'-N,4'-C-oxomethylenethymidine (2e: R = iPr). By following the general procedure 1, using 2-iodopropane as an alkyl halide, 2e was obtained in quant. as a white amorphous solid.

[α]$_D^{23}$ +57.2 (c 1.000, CHCl$_3$). IR (KBr): 3064, 3031, 2927, 2873, 1728, 1708, 1666, 1455, 1275 cm^{-1}. ^{1}H NMR (400 MHz, CDCl$_3$) δ: 1.18 (3H, d, J = 7 Hz), 1.31 (3H, d, J = 7 Hz), 1.64 (3H, s), 3.94, 4.10 (2H, AB, J = 12 Hz), 4.07 (1H, s), 4.28 (1H, s), 4.36–4.47 (1H, m), 4.50, 4.54 (2H, AB, J = 11.5 Hz), 4.58, 4.63 (2H, AB, J = 11.5 Hz), 4.71 (2H, s), 5.37 (1H, s), 5.46, 5.49 (2H, AB, J = 9.5 Hz), 7.18–7.39 (15H, m), 7.54 (1H, s). ^{13}C NMR (100.53 MHz, CDCl$_3$) δ: 12.9, 20.6, 21.1, 42.6, 58.9, 63.2, 70.1, 72.2, 72.2, 73.7, 78.2, 86.1, 88.0, 109.6, 127.3, 127.4, 127.5, 127.6, 127.6, 127.9, 128.1, 128.2, 128.2, 128.4, 129.4, 133.8, 136.2, 137.4, 137.7, 150.5, 163.2, 169.4. MS (FAB): m/z 626 [M + H]$^+$. HRMS (FAB): calcd for C$_{36}$H$_{40}$N$_3$O$_7$ [M + H]$^+$: 626.2866. Found: 626.2869.

(2'R)-3',5'-Di-O-benzyl-N^3-benzyloxymethyl-2'-benzylamino-2'-N,4'-C-oxomethylenethymidine (2f: R = Bn). By following the general procedure 1, using bromomethylbenzene as an alkyl halide, 2f was obtained in quant. as a white amorphous solid.

[α]$_D^{23}$ +17.1 (c 1.000, CHCl$_3$). IR (KBr): 3064, 3030, 2871, 1728, 1665, 1454, 1277 cm^{-1}. ^{1}H NMR (300 MHz, CDCl$_3$) δ: 1.60 (3H, s), 3.98, 4.12 (2H, AB, J = 12 Hz), 4.20, 4.26 (2H, AB, J = 11 Hz), 4.21, 4.85 (2H, AB, J = 15 Hz), 4.58, 4.65 (2H, AB, J = 11.5 Hz), 4.67 (2H, s), 5.34 (1H, s), 5.39, 5.45 (2H, AB, J = 9.5 Hz), 7.02–7.36 (20H, m), 7.48 (2H, s). ^{13}C NMR (100 MHz, CDCl$_3$) δ: 13.0, 45.1, 61.9, 63.2, 70.3, 72.3, 72.4, 74.0, 77.8, 85.0, 87.5, 109.9, 127.5, 127.7, 127.8, 128.0, 128.1, 128.1, 128.3, 128.4, 128.6, 128.6, 128.8, 133.9, 135.8, 136.2, 137.5, 137.8, 140.0, 150.5, 151.6, 163.3, 170.5. MS (FAB): m/z 674 [M + H]$^+$.

HRMS (FAB): calcd for C$_{40}$H$_{40}$N$_3$O$_7$ [M + H]$^+$: 674.2866. Found: 674.2841.

(2'R)-3',5'-Di-O-benzyl-N^3-benzyloxymethyl-2'-phenethylamino-2'-N,4'-C-oxomethylenethymidine (2g: R = CH$_2$CH$_2$Ph). By following the general procedure 1, using 2-bromoethylbenzene as an alkyl halide, 2g was obtained in 43% as a white amorphous solid.

[α]$_D^{24}$ +0.2 (c 0.320, CHCl$_3$). IR (KBr): 3029, 2930, 1722, 1701, 1667, 1453, 1274 cm^{-1}. ^{1}H NMR (300 MHz, CDCl$_3$) δ: 1.62 (3H, s), 2.82–3.02 (2H, m), 3.52–3.75 (2H, m), 3.94, 4.08 (2H, AB, J = 12 Hz), 4.02 (1H, s), 4.12 (1H, s), 4.44 (2H, s), 4.58, 4.63 (2H, AB, J = 11.5 Hz), 4.70 (2H, s), 5.29 (1H, s), 5.44, 5.48 (2H, AB, J = 9.5 Hz), 7.14–7.40 (20H, m), 7.49 (1H, s). ^{13}C NMR (100.53 MHz, CDCl$_3$) δ: 13.0, 34.7, 43.1, 63.3, 63.3, 70.3, 72.4, 72.5, 74.0, 78.3, 85.3, 87.5, 110.0, 126.7, 127.7, 127.7, 127.8, 128.1, 128.3, 128.3, 128.6, 128.6, 128.7, 133.9, 136.4, 137.5, 137.8, 137.9, 150.6, 163.3, 170.7. MS (FAB): m/z 688 [M + H]$^+$. HRMS (FAB): calcd for C$_{41}$H$_{42}$N$_3$O$_7$ [M + H]$^+$: 688.3023. Found: 688.3015.

General procedure 2 (synthesis of compound 3). To the solution of 2 (1.0 equiv.) in THF or methanol (0.1 M) was added 20% palladium on carbon (1.0 w/w) and the reaction vessel was degassed several times with hydrogen. The reaction mixture was stirred under a hydrogen atmosphere for 1–5 h at room temperature. After completion of the reaction, the reaction solution was filtered using filter paper and washed thoroughly with hot methanol. After evaporation of solvents, the product was dissolved with methanol (0.3 M) and 28% ammonia solution (0.3 M) was added and the solution was stirred at room temperature. After 5 min, the product was concentrated to afford S1 as a white solid.

To the solution of S1 in anhydrous pyridine (0.1 M) was added DMTrCl (1.3 equiv.) and the solution was stirred at room temperature. After stirring for 1–19 h, ice-cold water was added and the product was extracted with ethyl acetate. The organic phase was washed with brine, dried (Na$_2$SO$_4$), and concentrated. The product was purified by flash column chromatography (n-hexane–ethyl acetate = 1 : 1 or 1 : 3) to afford 3 as a white amorphous solid.

(2'R)-5'-O-(4,4'-Dimethoxytrityl)-2'-ethylamino-2'-N,4'-C-oxo-methylenethymidine (3c: R = Et). By following the general procedure 2, 3c was obtained in 45% (for 2 steps) as a white amorphous solid.

[α]$_D^{25}$ +12.9 (c 1.000, CHCl$_3$). IR (KBr): 3087, 2967, 2872, 1729, 1698, 1665, 1509, 1464 cm^{-1}. ^{1}H NMR (300 MHz, CDCl$_3$) δ: 1.16 (3H, t, J = 7 Hz), 1.62 (3H, s), 3.23–3.55 (2H, m), 3.63, 3.84 (2H, AB, J = 11.5 Hz), 3.74 (6H, s), 4.10 (1H, s), 4.24 (1H, s), 4.51 (1H, s), 5.39 (1H, s), 6.79–6.83 (4H, m), 7.13–7.45 (9H, m), 7.81 (1H, s), 10.33 (1H, s). ^{13}C NMR (100.53 MHz, CDCl$_3$) δ: 12.4, 13.4, 36.5, 55.1, 56.3, 64.9, 72.6, 85.3, 86.6, 88.8, 110.5, 112.9, 113.2, 127.0, 127.6, 127.8, 127.9, 129.0, 130.0, 135.1, 135.4, 144.3, 150.2, 158.4, 164.6, 170.5. MS (FAB): m/z 636 [M + Na]$^+$. HRMS (FAB): calcd for C$_{34}$H$_{35}$N$_3$O$_8$Na [M + Na]$^+$: 636.2322. Found: 636.2312.

(2'R)-5'-O-(4,4'-Dimethoxytrityl)-2'-propylamino-2'-N,4'-C-oxo-methylenethymidine (3d: R = nPr). By following the general

procedure 2, **3d** was obtained in 96% (for 2 steps) as a white amorphous solid.

$[\alpha]_D^{26}$ +33.1 (c 1.000, CHCl$_3$). IR (KBr): 3384, 3021, 2838, 1704, 1699, 1509, 1254 cm^{-1}. ^{1}H NMR (300 MHz, CDCl$_3$) δ: 1.17 (3H, t,J = 7 Hz), 1.62 (3H, s), 3.34–3.58 (2H, m), 3.61, 3.90 (2H, AB, J = 12 Hz), 3.91–3.98 (2H, m), 3.88 (6H, s), 4.28 (1H, s), 4.53 (1H, d, J = 7 Hz), 5.50 (1H, s), 6.83–6.85 (4H, m), 7.23–7.36 (7H, m), 7.44 (2H, d,J = 7 Hz), 7.82 (1H, s), 9.40 (1H, s). ^{13}C NMR (75 MHz, CDCl$_3$) δ: 11.2, 12.5, 21.7, 43.6, 55.2, 56.5, 65.2, 72.8, 85.2, 86.9, 88.6, 110.7, 113.3, 113.4, 127.1, 127.9, 128.1, 130.0, 135.1, 135.3, 144.3, 150.1, 158.6, 164.3, 170.6. MS (FAB): m/z 650 [M + Na]$^+$. HRMS (FAB): calcd for C$_{35}$H$_{37}$N$_3$O$_8$Na [M + Na]$^+$: 650.2478. Found: 650.2508.

(2'R)-5'-O-(4,4'-Dimethoxytrityl)-2'-isopropylamino-2'-N,4'-C-oxomethylenethymidine (3e: R = iPr). By following the general procedure 2, **3e** was obtained in 78% (for 2 steps) as a white amorphous solid.

$[\alpha]_D^{23}$ −3.83 (c 1.000, CHCl$_3$). IR (KBr): 3366, 3190, 2968, 2836, 1704, 1686, 1509, 1249 cm^{-1}. ^{1}H NMR (300 MHz, CDCl$_3$) δ: 1.17 (3H, d,J = 6.5 Hz), 1.28 (3H, d,J = 6.5 Hz), 1.69 (3H, s), 2.54 (1H, s), 3.59, 3.92 (2H, AB, J = 12 Hz), 3.77 (6H, s), 4.28 (1H, s), 4.28–4.37 (1H, m), 4.40 (1H, s), 5.37 (1H, s), 6.82–6.84 (4H, m), 7.20–7.36 (7H, m), 7.44 (2H, d,J = 7 Hz), 7.79 (1H, s), 9.65 (1H, s). ^{13}C NMR (100.53 MHz, CDCl$_3$): δ 12.5, 20.5, 21.1, 42.8, 55.2, 56.5, 61.5, 72.9, 86.0, 86.9, 89.2, 110.6, 113.3, 113.4, 127.1, 127.9, 128.1, 130.0, 135.2, 135.3, 144.4, 150.1, 158.6, 164.3, 169.4. MS (FAB): m/z 650 [M + Na]$^+$. HRMS (FAB): calcd for C$_{35}$H$_{37}$N$_3$O$_8$Na [M + Na]$^+$: 650.2478. Found: 650.2490.

(2'R)-5'-O-(4,4'-Dimethoxytrityl)-2'-benzylamino-2'-N,4'-C-oxomethylenethymidine (3f: R = Bn). By following the general procedure 2, **3f** was obtained in 90% (for 2 steps) as a white amorphous solid.

$[\alpha]_D^{25}$ +3.8 (c 1.000, CHCl$_3$). IR (KBr): 3063, 2967, 2837, 1686, 1607, 1509, 1249 cm^{-1}. ^{1}H NMR (300 MHz, CDCl$_3$) δ: 1.57 (3H, s), 3.67, 3.88 (2H, AB,J = 12 Hz), 3.74 (6H, s), 4.21 (1H, s), 4.44 (1H, s), 4.47, 4.52 (2H, AB, J = 15 Hz), 5.13 (1H, s), 6.79–6.83 (4H, m), 7.14–7.34 (7H, m), 7.39–7.44 (2H, d, J = 7 Hz), 7.74 (1H, s), 9.97 (1H, s). ^{13}C NMR (75 MHz, CDCl$_3$): δ 12.5, 45.6, 55.2, 56.5, 65.1, 72.4, 84.7, 86.8, 88.7, 110.6, 113.0, 113.3, 127.1, 127.9, 128.0, 128.7, 128.8, 130.0, 135.1, 135.2, 135.7, 144.3, 150.1, 158.6, 164.4, 170.7. MS (FAB): m/z 698 [M + Na]$^+$. HRMS (FAB): calcd for C$_{39}$H$_{37}$N$_3$O$_8$Na [M + Na]$^+$: 698.2478. Found: 698.2484.

(2'R)-5'-O-(4,4'-Dimethoxytrityl)-2'-phenethyl amino-2'-N,4'-C-oxomethylenethymidine (3g: R = CH$_2$CH$_2$Ph). By following the general procedure 2, **3g** was obtained in 84% (for 2 steps) as a white amorphous solid.

$[\alpha]_D^{21}$ +4.6 (c 0.400, CHCl$_3$). IR (KBr): 3190, 2958, 2929, 1721, 1694, 1672, 1509, 1270 cm^{-1}. ^{1}H NMR (300 MHz, CDCl$_3$) δ: 1.67 (3H, d,J = 8.5 Hz), 2.93–3.01 (2H, m), 3.56–3.66 (1H, m), 3.58, 3.87 (2H, AB,J = 12 Hz), 3.81 (7H, m), 4.07 (1H, s), 4.22 (1H, m), 4.34 (1H, s), 5.30 (1H, s), 6.83–7.85 (4H, m), 7.16–7.54 (14H, m), 7.72 (1H, d, J = 8.5 Hz), 8.61 (1H, s). ^{13}C NMR (75 MHz, CDCl$_3$) δ: 13.0, 34.7, 43.1, 63.3, 63.3, 70.3, 72.4, 72.5, 74.0, 78.3, 85.3, 87.5, 109.9, 126.7, 127.7, 127.7, 127.8, 128.1, 128.3, 128.3, 128.6, 128.6, 128.7, 133.9, 136.4, 137.5, 137.8,

137.9, 150.6, 163.3, 170.7. MS (FAB): m/z 712 [M + Na]$^+$. HRMS (FAB): calcd for C$_{40}$H$_{39}$N$_3$O$_8$Na [M + Na]$^+$: 712.2635. Found: 712.2631.

General procedure 3 (synthesis of compound 4). To the solution of **3** (1.0 equiv.) in anhydrous MeCN–THF (3 : 1, 0.1 M) were added N,N-diisopropylammonium tetrazolide (0.75 equiv.) and 2-cyanoethyl-N,N,N',N'-tetraisopropylphosphorodiamidite (1.2 equiv.). After stirring at room temperature for 9 h–19 h, ice-cold water was added and the product was extracted with ethyl acetate. The organic phase was washed with brine, dried (Na$_2$SO$_4$), and concentrated. The product was purified by flash column chromatography (0.05 eq. of triethylamine in n-hexane–ethyl acetate = 1 : 1) to afford **4c** (R = Et: 39 mg, 77%) as a white amorphous solid.

(2'R)-3'-O-[2-Cyanoethoxy(disopropylamino)phosphino]-5'-O-(4,4'-dimethoxytrityl)-2'-ethylamino-2'-N,4'-C-oxomethylenethymidine (4c: R = Et). By following the general procedure 3, **4c** was obtained in 77% as a white amorphous solid.

M.p. 100–103 °C (CH$_2$Cl$_2$–hexane). ^{31}P NMR (161.83 MHz, CDCl$_3$) δ: 149.2, 150.3. MS (FAB): m/z 814 [M + H]$^+$. HRMS (FAB): calcd for C$_{43}$H$_{53}$N$_5$O$_9$P [M + H]$^+$: 814.3581. Found: 814.3588.

(2'R)-3'-O-[2-Cyanoethoxy(disopropylamino)phosphino]-5'-O-(4,4'-dimethoxytrityl)-2'-propylamino-2'-N,4'-C-oxomethylenethymidine (4d: R = nPr). By following the general procedure 3, **4d** was obtained in 88% as a white amorphous solid.

M.p. 83–86 °C (CH$_2$Cl$_2$–hexane). ^{31}P NMR (161.83 MHz, CDCl$_3$) δ: 149.8, 150.2. MS (FAB): m/z 828 [M + H]$^+$. HRMS (FAB): calcd for C$_{44}$H$_{55}$N$_5$O$_9$P [M + H]$^+$: 828.3737. Found: 828.3745.

(2'R)-3'-O-[2-Cyanoethoxy(disopropylamino)phosphino]-5'-O-(4,4'-dimethoxytrityl)-2'-isopropylamino-2'-N,4'-C-oxomethylenethymidine (4e: R = iPr). By following the general procedure 3, **4e** was obtained in 32% as a white amorphous solid.

M.p. 101–104 °C (CH$_2$Cl$_2$–hexane). ^{31}P NMR (161.83 MHz, CDCl$_3$) δ: 149.5, 151.3. MS (FAB): m/z 828 [M + H]$^+$. HRMS (FAB): calcd for C$_{44}$H$_{55}$N$_5$O$_9$P [M + H]$^+$: 828.3737. Found: 828.3729.

(2'R)-3'-O-[2-Cyanoethoxy(disopropylamino)phosphino]-5'-O-(4,4'-dimethoxytrityl)-2'-benzylamino-2'-N,4'-C-oxomethylenethymidine (4f: R = Bn). By following the general procedure 3, **4f** was obtained in 61% as a white amorphous solid.

M.p. 99–101 °C (CH$_2$Cl$_2$–hexane). ^{31}P NMR (161.83 MHz, CDCl$_3$) δ: 150.0, 150.2. MS (FAB): m/z 876 [M + H]$^+$. HRMS (FAB): calcd for C$_{48}$H$_{55}$N$_5$O$_9$P [M + H]$^+$: 876.3737. Found: 876.3735.

(2'R)-3'-O-[2-Cyanoethoxy(disopropylamino)phosphino]-5'-O-(4,4'-dimethoxytrityl)-2'-phenethylamino-2'-N,4'-C-oxomethylenethymidine (4g: R = CH$_2$CH$_2$Ph). By following the general procedure 3, **4g** was obtained in 48% as a white amorphous solid.

M.p. 98–101 °C (CH$_2$Cl$_2$–hexane). ^{31}P NMR (161.83 MHz, CDCl$_3$) δ: 149.6, 150.8. MS (FAB): m/z 890 [M + H]$^+$. HRMS (FAB): calcd for C$_{49}$H$_{57}$N$_5$O$_9$P [M + H]$^+$: 890.3894. Found: 890.3909.

Synthesis, purification and characterization of oligonucleotides

Synthesis of 0.2 μmol scale of oligonucleotides **ON-6-44** modified with AmNA[*N*-Me] was performed using Oligonucleotide Synthesizer (Gene Design, ns-8) according to the standard phosphoramidite protocol with Activator 42™ (Proligo) as the activator. Dry MeCN was used to dissolve AmNA[*N*-R]. The standard synthesis cycle was used for assembly of the reagents and synthesis of the oligonucleotides, except that the coupling time was extended to 16 minutes for AmNA[*N*-R] monomers. (The coupling time for AmNA[*N*-Me] was 32 seconds.) The synthesis was carried out in trityl on mode and was treated with concentrated ammonium hydroxide at room temperature for 1 h to cleave the synthesized oligonucleotides from the solid support. The oligonucleotides were initially purified by Sep-pack Plus C_{18} Environmental Cartridge. The separated oligonucleotides were further purified by reverse-phase HPLC with Waters Xbridge™ Shield RP_{18} 2.5 μm (10 mm × 50 mm) columns with a linear gradient of MeCN (7–13% over 42 min for **ON-3-6**, **ON-11**, **ON-12**, **ON-16**, 8–15% over 42 min for **ON-7**, **ON-8**, 13–40% over 42 min for **ON-13**, **ON-17**) in 0.1 M triethylammonium acetate (pH 7.0). The oligonucleotides were analyzed for purity by HPLC and characterized by MALDI-TOF mass spectroscopy.

UV melting experiments and melting profiles

The UV melting experiments were carried out using a Shimadzu UV-1650 spectrometer equipped with a T_m analysis accessory. Equimolecular amounts of the target RNA or DNA strand and oligonucleotide were dissolved in buffer A (10 mM phosphate buffer at pH 7.2 containing 100 mM NaCl) to give a final strand concentration of 4 μM. The samples were annealed by heating at 95 °C followed by slow cooling to room temperature. The melting profile was recorded at 260 nm from 0 to 70 °C (for **ON-3-8**), from 5 to 100 °C (for **ON-11-13**, **16**, **17**) at a scan rate of 0.5 °C min^{-1}. The T_m was calculated as the temperature of the half-dissociation of the formed duplexes, determined by the midline of the melting curve.

Enzymatic digestion study

The sample solutions were prepared by dissolving 0.75 μmol of oligonucleotides in 50 mM Tris-HCl buffer (pH 8.0) containing 10 mM $MgCl_2$. To each sample solution, 0.175 μL *Crotalus adamanteus* venom phosphodiesterase (CAVP) was added and the cleavage reaction was carried out at 37 °C. A portion of each reaction mixture was removed at timed intervals and heated to 90 °C for 5 min to deactivate the nuclease. Aliquots of the timed samples were analyzed by RP-HPLC to evaluate the amount of intact oligonucleotides remaining. The percentage of intact oligonucleotide in each sample was calculated and plotted against the digestion time to obtain a degradation curve with time (Fig. S5†).

In vivo knockdown study

All animal procedures were performed in accordance with the guidelines of the Animal Care Ethics Committee of the National Cerebral and Cardiovascular Center Research Institute (Osaka, Japan). All animal studies were approved by an Institutional Review Board. C57BL/6J mice were obtained from CLEA Japan. All mice were male, and studies were initiated when animals were 8 weeks of age. Mice (*n* = 3 per arm) were maintained on a 12 h light/12 h dark cycle and fed *ad libitum*. Mice were fed a normal chow (CE-2, CLEA Japan) for 2 weeks before and during treatment. Mice received single treatment of saline-formulated AONs intravenously. At the time of sacrifice after 72 hours of injection, mice were subjected to blood collection from tail veins and then anesthetized with isoflurane (Forane, Abbott Japan) under an overnight fasting condition. Livers were harvested and snap frozen until subsequent analysis. Whole blood was collected and subjected to serum separation for subsequent analysis.

mRNA quantification

Frozen liver tissue was collected in a 2 mL tube with 1 mL of TRIzol Reagent (Life Technologies, Japan) and a zirconia ball (∅ 5 mm, Irie) and mechanically homogenized for 2 min at 30 oscillations per second by a TissueLyser II apparatus (Qiagen). Total RNA was isolated from the resulting suspensions according to the manufacturer's procedure. Gene expression was evaluated by a 2-step quantitative RT-PCR method. Reverse-transcription of RNA samples was performed by using a High Capacity cDNA Reverse-Transcription Kit (Applied Biosystems), and quantitative PCR was performed by TaqMan(R) Fast Universal PCR Master Mix (Applied Biosystems). The mRNA levels of target genes were normalized to the GAPDH mRNA level. For murine apoC-III and GAPDH mRNA quantitation, TaqMan Gene Expression Assay IDs of Mm00445670_m1 and Mm99999915_g1 were used.

ELISA method for AON quantification in liver

Materials and reagents. The template DNA was a 25-mer DNA (5′-gaa tag cga taa taa agc tgg ata a-3′), which is complementary to **ON-9S** to **ON-15S**, with biotin at the 3′-end. The ligation probe DNA was a 9-mer DNA (5′-tcgctattc-3′) with phosphate at the 5′-end and digoxigenin at the 3′-end. The template DNA and the ligation probe DNA were purchased from Japan Bio Service. Reacti-Bind NeutrAvidin-coated polystyrene strip plates were purchased from Thermo Fisher Scientific (Nunc immobilizer streptavidin F96 white, 436015). The template DNA solution (100 nM) was prepared in hybridization buffer containing 60 mM Na_2HPO_4 (pH 7.4), 0.9 M NaCl, and 0.24% Tween 20. The ligation probe DNA solution (200 nM) was prepared in 1.5 units per well of T4 DNA ligase (TaKaRa) with 66 mM Tris-HCl (pH 7.6), 6.6 mM $MgCl_2$, 10 mM DTT and 0.1 mM ATP.

The washing buffer used throughout the assay contained 25 mM Tris-HCl (pH 7.2), 0.15 M NaCl and 0.1% Tween 20. Anti-digoxigenin-AP antibody (Fab fragments conjugated with

alkaline phosphatase) was obtained from Roche Diagnostics. A 1 : 2000 dilution of the antibody with 1 : 10 super block buffer in TBS (Pierce) was used in the assay. The alkaline phosphatase luminous substrate was prepared in 250 µM CDP-Star (Roche) with 100 mM Tris-HCl (pH 7.6) and 100 mM NaCl.

Assay procedures. Frozen liver tissue was collected in a 2 mL tube with 1 mL of PBS and a zirconia ball (∅ 5 mm, Irie) and mechanically homogenized for 2 min at 30 oscillations per second by a TissueLyser II apparatus (Qiagen). Total protein concentrations were measured using a detergent compatible assay kit (Bio-Rad) and adjusted to 8 mg L^{-1} with PBS. The assay was performed at the concentration range of 128 pM to 1000 nM in duplicate. For the standard curve, 7 standard solutions were prepared. To AON-untreated mice liver homogenates were added **ON-10S, ON-11S, ON-12S, ON-13S, ON-14S,** and **ON-15S** solutions to prepare 7 standard samples at a range of 128 pM to 1000 nM. Next, the template DNA solution (100 µL) and standard solution (10 µL) or liver homogenates (10 µL) containing **ON-10S, ON-11S, ON-12S, ON-13S, ON-14S,** and **ON-15S** were added to Reacti-Bind Neutr Avidin-coated polystyrene strip 96-well plates and incubated at 37 °C for 1 h to allow the binding of biotin to streptavidin-coated wells and hybridization. After hybridization, the plate was washed three times with 200 µL of washing buffer. Then, ligation probe DNA solution (100 µL) was added, and the plate was incubated at room temperature (15 °C) for 3 h. The plate was then washed three times with the washing buffer. Subsequently, 200 µL of a 1 : 2000 dilution of anti-digoxigenin-AP was added, and the plate was incubated at 37 °C for 1 h. After washing three times with the washing buffer, the CDP-Star solution was added to the plate, and finally the luminescence intensity was determined by using a Centro XS^3 luminometer (Berthold) one second after the addition of CDP-Star. The linear range of 128 pM to 1000 nM in this ELISA system was determined as $r > 0.97$.

Serum chemistry

Serum from the blood collected from the inferior vena cava upon sacrifice was subjected to serum chemistry. Assay kits (WAKO) were used to measure serum levels of aspartate aminotransferase (AST) and alanine aminotransferase (ALT), which are biomarkers for hepatic toxicity.

Statistics

Statistical comparisons were performed by Dunnett's multiple comparison tests. $*P < 0.05$, $**P < 0.01$, and $***P < 0.001$ were considered to be statistically significant in all cases. N.S. indicates no statistical significance.

Acknowledgements

Notes and references

1 (a) E. R. Rayburn and R. Zhang, *Drug Discovery Today*, 2008, **13**, 513; (b) T. Yamamoto, M. Nakatani, K. Narukawa and S. Obika, *Future Med. Chem.*, 2011, **3**, 339.

2 (a) S. Obika, D. Nanbu, Y. Hari, K. Morio, Y. In, T. Ishida and T. Imanishi, *Tetrahedron Lett.*, 1997, **38**, 8735; (b) S. K. Singh and J. Wengel, *Chem. Commun.*, 1998, 1247.

3 (a) T. Yamamoto, M. Harada-Shiba, M. Nakatani, S. Wada, H. Yasuhara, K. Narukawa, K. Sasaki, M. A. Shibata, H. Torigoe, T. Yamaoka, T. Imanishi and S. Obika, *Mol. Ther. Nucleic acids*, 2012, **1**, e22; (b) K. Fluiter, A. L. ten Asbroek, M. B. de Wissel, M. E. Jakobs, M. Wissenbach, H. Olsson, O. Olsen, H. Oerum and F. Baas, *Nucleic Acids Res.*, 2003, **31**, 953; (c) K. Fluiter, M. Frieden, J. Vreijling, C. Rosenbohm, M. B. De Wissel, S. M. Christensen, T. Koch, H. Orum and F. Baas, *ChemBioChem*, 2005, **6**, 1104; (d) E. M. Straarup, N. Fisker, M. Hedtjarn, M. W. Lindholm, C. Rosenbohm, V. Aarup, H. F. Hansen, H. Orum, J. B. Hansen and T. Koch, *Nucleic Acids Res.*, 2010, **38**, 7100.

4 (a) R. S. Geary, E. Wancewicz, J. Matson, M. Pearce, A. Siwkowski, E. Swayze and F. Bennett, *Biochem. Pharmacol.*, 2009, **78**, 284; (b) M. J. Graham, S. T. Crooke, D. K. Monteith, S. R. Cooper, K. M. Lemonidis, K. K. Stecker, M. J. Martin and R. M. Crooke, *J. Pharmacol. Exp. Ther.*, 1998, **286**, 447.

5 (a) E. E. Swayze, A. M. Siwkowski, E. V. Wancewicz, M. T. Migawa, T. K. Wyrzykiewicz, G. Hung, B. P. Monia and C. F. Bennett, *Nucleic Acids Res.*, 2007, **35**, 687; (b) E. P. van Poelgeest, R. M. Swart, M. G. Betjes, M. Moerland, J. J. Weening, Y. Tessier, M. R. Hodges, A. A. Levin and J. Burggraaf, *Am. J. Kidney Dis.*, 2013, **62**, 796.

6 (a) O. Nakagawa, X. Ming, L. Huang and R. L. Juliano, *J. Am. Chem. Soc.*, 2010, **132**, 8848; (b) T. P. Prakash, M. J. Graham, J. H. Yu, R. Carty, A. Low, A. Chappell, K. Schmidt, C. G. Zhao, M. Aghajan, H. F. Murray, S. Riney, S. L. Booten, S. F. Murray, H. Gaus, J. Crosby, W. F. Lima, S. L. Guo, B. P. Monia, E. E. Swayze and P. P. Seth, *Nucleic Acids Res.*, 2014, **42**, 8796; (c) J. Winkler, *Ther. Delivery*, 2013, **4**, 791.

7 (a) S. M. A. Rahman, S. Seki, S. Obika, H. Yoshikawa, K. Miyashita and T. Imanishi, *J. Am. Chem. Soc.*, 2008, **130**, 4886; (b) P. P. Seth, A. Siwkowski, C. R. Allerson,

G. Vasquez, S. Lee, T. P. Prakash, E. V. Wancewicz, D. Witchell and E. E. Swayze, *J. Med. Chem.*, 2009, **52**, 10; (c) T. P. Prakash, A. Siwkowski, C. R. Allerson, M. T. Migawa, S. Lee, H. J. Gaus, C. Black, P. P. Seth, E. E. Swayze and B. Bhat, *J. Med. Chem.*, 2010, **53**, 1636; (d) P. P. Seth, C. R. Allerson, A. Berdeja, A. Siwkowski, P. S. Pallan, H. Gaus, T. P. Prakash, A. T. Watt, M. Egli and E. E. Swayze, *J. Am. Chem. Soc.*, 2010, **132**, 14942; (e) P. P. Seth, G. Vasquez, C. A. Allerson, A. Berdeja, H. Gaus, G. A. Kinberger, T. P. Prakash, M. T. Migawa, B. Bhat and E. E. Swayze, *J. Org. Chem.*, 2010, **75**, 1569; (f) K. Miyashita, S. M. A. Rahman, S. Seki, S. Obika and T. Imanishi, *Chem. Commun.*, 2007, 3765.

8 J. Lietard and C. J. Leumann, *J. Org. Chem.*, 2012, **77**, 4566.

9 A. Yahara, A. R. Shrestha, T. Yamamoto, Y. Hari, T. Osawa, M. Yamaguchi, M. Nishida, T. Kodama and S. Obika, *Chem-BioChem*, 2012, **13**, 2513.

10 (a) M. W. Johannsen, L. Crispino, M. C. Wamberg, N. Kalra and J. Wengel, *Org. Biomol. Chem.*, 2011, **9**, 243; (b) S. K. Singh, R. Kumar and J. Wengel, *J. Org. Chem.*, 1998, **63**, 6078; (c) M. D. Sorensen, M. Petersen and J. Wengel, *Chem. Commun.*, 2003, 2130.

11 K. Mori, T. Kodama, T. Baba and S. Obika, *Org. Biomol. Chem.*, 2011, **9**, 5272.

12 (a) Y. Mitsuoka, T. Kodama, R. Ohnishi, Y. Hari, T. Imanishi and S. Obika, *Nucleic Acids Res.*, 2009, **37**, 1225; (b) M. Nishida, T. Baba, T. Kodama, A. Yahara, T. Imanishi and S. Obika, *Chem. Commun.*, 2010, **46**, 5283; (c) K. Morita, M. Takagi, C. Hasegawa, M. Kaneko, S. Tsutsumi, J. Sone, T. Ishikawa, T. Imanishi and M. Koizumi, *Bioorg. Med. Chem.*, 2003, **11**, 2211; (d) Y. Liu, J. Xu, M. Karimiahmadabadi, C. Zhou and J. Chattopadhyaya, *J. Org. Chem.*, 2010, **75**, 7112; (e) A. R. Shrestha, Y. Kotobuki, Y. Hari and S. Obika, *Chem. Commun.*, 2014, **50**, 575.

13 M. Egli, G. Minasov, M. Teplova, R. Kumar and J. Wengel, *Chem. Commun.*, 2001, 651.

14 T. Yamamoto, S. Obika, M. Nakatani, H. Yasuhara, F. Wada, E. Shibata, M. A. Shibata and M. Harada-Shiba, *Eur. J. Pharmacol.*, 2014, **723**, 353.

15 T. Yamamoto, N. Fujii, H. Yasuhara, S. Wada, F. Wada, N. Shigesada, M. Harada-Shiba and S. Obika, *Nucleic Acid Ther.*, 2014, **24**, 283.

16 (a) T. Yamamoto, M. Harada-Shiba, M. Nakatani, S. Wada, H. Yasuhara, K. Narukawa, K. Sasaki, M. A. Shibata, H. Torigoe, T. Yamaoka, T. Imanishi and S. Obika, *Mol. Ther. Nucleic Acids*, 2012, **1**; (b) R. Z. Yu, B. Baker, A. Chappell, R. S. Geary, E. Cheung and A. A. Levin, *Anal. Biochem.*, 2002, **304**, 19.

Removal of Plasma Mature and Furin-Cleaved Proprotein Convertase Subtilisin/Kexin 9 by Low-Density Lipoprotein-Apheresis in Familial Hypercholesterolemia: Development and Application of a New Assay for PCSK9

Mika Hori, Mitsuaki Ishihara, Yumiko Yuasa, Hisashi Makino, Koji Yanagi, Tamiko Tamanaha, Ichiro Kishimoto, Takeshi Kujiraoka, Hiroaki Hattori, and Mariko Harada-Shiba

Department of Molecular Innovation in Lipidology (M.H., Y.Y., M.H-S.), National Cerebral and Cardiovascular Center Research Institute, 5-7-1 Fujishirodai, Suita, Osaka 565-8565, Japan; Advanced Medical Technology and Development Division (M.I., T.K., H.H.), BML, Inc., 1361-1 Matoba, Kawagoe, Saitama 350-1101, Japan; Department of Endocrinology and Metabolism (H.M., T.T., I.K.), National Cerebral and Cardiovascular Center, 5-7-1 Fujishirodai, Suita, Osaka 565-8565, Japan; and Department of Cardiology (K.Y.), Kenporen Osaka Central Hospital, Umeda 3-3-30, Kita-ku, Osaka 530-0001, Japan.

Context: Proprotein convertase subtilisin/kexin 9 (PCSK9) is known to be a good target to decrease LDL cholesterol (LDL-C) and two forms of PCSK9, mature and furin-cleaved PCSK9, circulate in blood. However, it has not been clarified whether and how the levels of each PCSK9 are affected by LDL-apheresis (LDL-A) treatment, a standard therapy in patients with severe forms of familial hypercholesterolemia (FH).

Objective: Our objective was to investigate the differences in LDL-A-induced reduction of mature and furin-cleaved PCSK9 between homozygous and heterozygous FH, and between dextran sulfate (DS) cellulose adsorption and double membrane (DM) columns and to clarify the mechanism of their removal.

Design: A sandwich ELISA to measure two forms of PCSK9s using monoclonal antibodies was developed. Using the ELISA, PCSK9 levels were quantified before and after LDL-A with DS columns in 7 homozygous and 11 heterozygous FH patients. A crossover study between the two column types was performed. The profiles of PCSK9s were analyzed after fractionation by gel filtration chromatography. Immunoprecipitation of apolipoprotein B (apoB) in FH plasma was performed.

Results: Both mature and furin-cleaved PCSK9s were significantly decreased by 55–56% in FH homozygotes after a single LDL-A treatment with DS columns, and by 46–48% or 48–56% in FH heterozygotes after treatment with DS or DM columns. The reduction ratios of LDL-C were strongly correlated with that of PCSK9 in both FH homozygotes and heterozygotes. In addition, more than 80% of plasma PCSK9s were in the apoB-deficient fraction and a significant portion of mature PCSK9 was bound to apoB, as shown by immunoprecipitation.

Conclusions: Both mature and furin-cleaved PCSK9s were removed by LDL-A in homozygous and heterozygous FH either by binding to apoB or by other mechanisms. The ELISA method to measure both forms of plasma PCSK9 would be useful for investigating physiological or pathological roles of PCSK9. (*J Clin Endocrinol Metab* **100: E41–E49, 2015**)

Abbreviations: DM, double membrane; DS, dextran sulfate; HDL, high-density lipoprotein; LDL, low-density lipoprotein; LDL-A, LDL-apheresis; LDL-C, LDL cholesterol; LDLR, low-density lipoprotein receptor; PCSK9, proprotein convertase subtilisin/kexin type 9; rh, recombinant human; TG, triglyceride.

Familial hypercholesterolemia (FH) is an inherited disorder caused by mutations in the low-density lipoprotein (LDL) receptor (LDLR), apolipoprotein B (apoB) or proprotein convertase subtilisin/kexin type 9 (PCSK9) (1, 2), and is characterized by high LDL cholesterol (LDL-C) levels leading to premature coronary artery disease (CAD). PCSK9, a serine protease, regulates plasma LDL-C levels by regulating degradation of LDLR (3, 4). It has also been reported that serum PCSK9 levels were significantly higher in FH patients than in controls (5), and were correlated with serum LDL-C levels (6).

PCSK9 encodes a 692-amino-acid protein composed of a signal peptide, a prodomain, catalytic, and C-terminal domains. It undergoes autocatalytic intramolecular processing to form a $\sim$14-kDa prodomain and a $\sim$60-kDa moiety with catalytic and C-terminal domains. Mature PCSK9 is composed of the prodomain, which is noncovalently attached to the catalytic domain. Another proprotein convertase, furin, cleaves PCSK9 at the Arg^{218}-Gln^{219} peptide bond, and the cleaved PCSK9 includes a $\sim$7-kDa domain, $\sim$14-kDa prodomain, and $\sim$53-kDa domain (furin-cleaved form) that lacks the Ser^{153}-Arg^{218} segment (7, 8). It has been reported that furin-cleaved PCSK9 has no activity (7–9) to regulate LDLR and serum LDL-C or less activity than mature PCSK9 (10). Thus, it is important to measure both forms of PCSK9 separately, in order to clarify the significance of furin-cleaved PCSK9. However, no specific method has been reported for quantifying furin-cleaved PCSK9, and thus the association of the ratio of each form of PCSK9 with various pathological or physiological conditions, such as primary hyperlipidemia, hyperlipidemia in type II diabetes, obesity, etc., has not been clarified.

LDL-apheresis (LDL-A) treatment is a standard therapy in homozygous and severe forms of heterozygous FH. In order to selectively remove LDL, LDL adsorption techniques using dextran sulfate (DS) cellulose adsorption columns and double membrane (DM) filtration methods were developed (11, 12). We and other colleagues have reported that LDL-A reduces not only atherogenic lipoproteins, but also various proteins including coagulation factors and C-reactive protein (CRP), in serum (13–15).

Recently, it has been reported that PCSK9 was eliminated by LDL-A treatment in 6 FH patients (16). However, in FH homozygotes, the serum PCSK9 levels have been reported to be unaffected by LDL-A (17). Thus, the difference in the treatment-induced reduction of PCSK9 between FH homozygotes and heterozygotes has not been clarified. In addition, the differences in the PCSK9 reduction between DS and DM columns and between the mature and furin-cleaved forms have not been clarified. In the present study, we use a novel sandwich ELISA to measure the mature and furin-cleaved forms of PCSK9 and show that both forms were removed by LDL-A treatment in FH homozygotes and heterozygotes. Furthermore, the mechanism of their removal is also discussed.

Materials and Methods

Detailed materials and methods are shown in the Supplemental Materials and Methods.

Patient characteristics

The subjects were 18 FH patients, including 7 homozygotes and 11 heterozygotes, who were receiving either regular or an initial LDL-A treatment at either the National Cerebral and Cardiovascular Center Hospital or Kenporen Osaka Central Hospital from March 2009 to October 2013. They were diagnosed with homozygous or heterozygous FH using previously described criteria (18, 19). Among the patients who had undergone genetic testing (n = 12), the majority were found to have LDLR gene mutations (n = 6; 50%), and one had mutations of both the LDLR and PCSK9 genes. One patient had homozygous forms of LDL receptor adaptor protein 1 (LDLRAP1) gene mutation, and 5 patients had no mutation on either the LDLR, PCSK9, or LDLRAP1 genes (42%) (20). The backgrounds of the patients are summarized in Supplemental Table 1. The protocol of this study was approved by the Ethics Review Committee of the National Cerebral and Cardiovascular Center (M20–26). Each patient gave written informed consent to participate in the study. All clinical investigations were conducted in accordance with the principles of the Declaration of Helsinki.

LDL-apheresis

For LDL-A treatment, an instrument (MA-03®; Kaneka) with a plasma filter (Sulflux; Kaneka) and two DS columns (Liposorber LA-15®; Kaneka) to adsorb apoB-containing lipoproteins were used. A crossover study between DS and DM columns was performed in 5 FH heterozygotes (patients No. 8, 10, 11, 12, 14 in Supplemental Table 1). LDL-A by DM columns was performed using an instrument (KPS-8800Ce; Asahi Kasei Medical Co., Ltd.) with a plasma separator (Plasmaflow OP-05W; Asahi Kasei Medical Co., Ltd.) and a plasma fractionator (Cascadeflow EC-50W; Asahi Kasei Medical Co., Ltd.).

Plasma sample collections and assays

Peripheral blood was collected from the blood removal line immediately before and after a single LDL-A procedure. Plasma levels of total cholesterol (TC), triglyceride (TG), and high-density lipoprotein (HDL)-C were measured using enzymatic methods (Sekisui Medical Co.) and an automated analyzer (Hitachi Labospect 008, Hitachi-Hitec). Plasma Lipoprotein(a) (Lp(a)) levels were measured using a latex agglutination method (Sekisui Medical Co.). LDL-C levels were calculated by the Friedewald formula. Apolipoproteins levels were determined by turbidimetric immunoassay (LSI Medience Coorporation).

Construction, expression, and purification of recombinant PCSK9 proteins

Human PCSK9 cDNA was obtained by RT-PCR from mRNA of HepG2 cells and a C-terminal His_6 tag was added as described

(21). Briefly, PCR was carried out for mature PCSK9 (1–692 aa), and Δ218PCSK9 (219–692 aa), which corresponds to the furin-cleaved PCSK9. The respective cDNAs were subcloned into the pEF321 mammalian expression vector to yield pEF321/PCSK9 or pEF321/Δ218PCSK9 vector. CHO-K1 cells stably transfected with each vector were cultured. The mature form of recombinant human (rh) PCSK9 (rhPCSK9) from the culture medium was partially purified. For rhΔ218PCSK9, transfectant cells were collected by trypsinization, and suspended in TBS containing 1% NP-40. After centrifugation of the cell suspension, the supernatant was collected and used as a calibrator for furin-cleaved PCSK9 ELISA.

Production of monoclonal antibodies against PCSK9

Balb/c mice were immunized using a DNA-based or standard immunization method with 25 μg purified rhPCSK9 (21), and spleen cells from mice were fused with Sp2/0 myeloma cells. The supernatants of hybridoma cells were screened by ELISA using plates coated with purified rhPCSK9 (100 ng/well) and by immunoblotting. The specificities of each monoclonal antibody (Mab) obtained by standard immunization (1FB) and by DNA-based immunization (B1G, B12E, and G12D), respectively, were confirmed by ELISA and immunoblotting against purified rhPCSK9.

Measurement of plasma mature and furin-cleaved PCSK9 concentrations

Plasma mature and furin-cleaved PCSK9s were measured by an ELISA using a specific combination of Mabs as previously described (Supplemental Figure 1) (21). The absorbance was measured at 450 nm with a microplate reader.

Gel filtration chromatography

Gel filtration chromatography was performed on an AKTA purifier system (GE Healthcare). Plasma samples of 2 homozygous and 6 heterozygous FH patients were injected into two connected Superose 6 (1.0 × 30; GE Healthcare) columns (22). Cholesterol or Lp(a) was measured in the fractions using a BIO-Lis24 analyzer (Tokyo Boeki Medical System, Ltd.) or a Mercodia Lp(a) ELISA (Mercodia AB) with two Mabs against Apo(a) in accordance with the manufacturers' instructions. PCSK9s in the collected fractions were measured using the ELISA as described above.

Co-immunoprecipitation of apoB from FH plasma

A 500 μL plasma sample was adjusted to a final concentration of 50 mM HEPES [pH 7.4], 2.5 mM magnesium chloride, 1% Triton X-100, 0.5% sodium deoxycholate and protease inhibitor cocktail in a final volume of 1 mL. Samples were rotated at 4°C for 30 min, then centrifuged at 15 000 rpm for 15 min. Co-immunoprecipitation experiments were performed using a Pierce Co-Immunoprecipitation Kit (Pierce) following the manufacturer's instructions. The supernatants were applied to columns containing 20 μg of monoclonal anti-apoB antibody (Santa Cruz Biotechnology Inc.) or 20 μg of purified IgG from a nonimmunized mouse (Santa Cruz Biotechnology Inc.). The immunoprecipitates were separated by SDS-PAGE, followed by immunoblotting with monoclonal anti-apoB antibody (R&D

Systems) or polyclonal PCSK9 antibody (R&D Systems). The bands were detected with ECL prime (GE Healthcare).

Statistical analysis

The statistical significance of differences between before and after LDL-A treatment was determined by the paired t-test. One-way ANOVA and Tukey's test were used to assess differences between groups. Spearman correlation analysis and linear regression were used to examine the relationship between PCSK9 reduction and LDL-C or HDL-C reduction. Values of $P < .05$ were considered to be statistically significant. All statistical analyses were carried out using the JMP software package (SAS Institute Inc.).

Results

Characterization of anti-PCSK9 Mabs

Purified rhPCSK9 was confirmed by SDS-PAGE followed by silver staining or by immunoblotting (Figure 1, A and B). The reactivity of Mabs to rhPCSK9 (mature form) was examined by SDS-PAGE under a nonreducing or reducing condition and by immunoblotting; Mabs 1FB, B1G, and B12E reacted with the 60-kDa mature PCSK9, while Mab G12D reacted with a 14-kDa prodomain of PCSK9 (Figure 1C). These three Mabs did not react with the mature segment of rhPCSK9 under a reducing condition. Similarly, the reactivity of all Mabs with native PCSK9 in human plasma was examined by immunoprecipitation. The 60-kDa mature PCSK9 and the 14-kDa prodomain of PCSK9 were co-immunoprecipitated with Mabs 1FB, B12E, and G12D, while the 53-kDa furin-cleaved PCSK9 alone was precipitated with Mab B1G (Figure 1, D and E).

Standardization of ELISA for the mature and furin-cleaved PCSK9s in plasma

We have established three different sandwich ELISAs specific for plasma total, mature and furin-cleaved PCSK9s (Supplemental Figure 1). Each system showed a dose-dependent response to purified rhPCSK9 or cell lysate of rhΔ218PCSK9 as well as to plasma samples, and the reactivity profiles were equivalent with both recombinant and plasma PCSK9 (Supplemental Figure 2). Calibration curves in the ELISA for total and mature PCSK9, rhPCSK9 protein, as a primary calibrator and rhPCSK9 culture medium, as a secondary calibrator were obtained (Supplemental Figure 3). Similarly, the calibration curve was made using dilutions of the cell lysate of rhΔ218PCSK9 for furin-cleaved PCSK9.

Changes of plasma lipids and apolipoproteins between before and after LDL-A with DS columns in FH homozygotes or heterozygotes

In FH homozygotes, a single procedure of LDL-A treatment with DS columns produced 57–78% reduction in
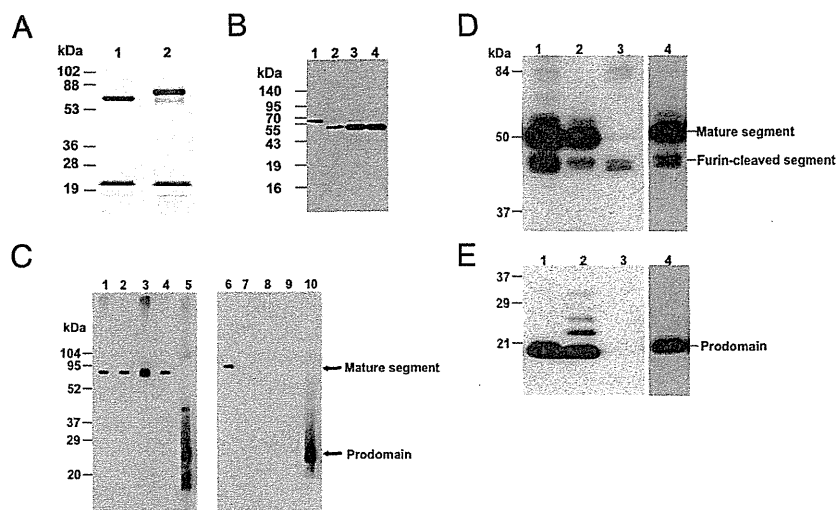
Figure 1. Characterization of recombinant PCSK9 and monoclonal antibodies to PCSK9. (A) Purified rhPCSK9 (0.75 μg) was analyzed by 5–20% SDS-PAGE under nonreducing (lane 1) and reducing (lane 2) conditions and visualized by silver staining. (B) Purified rhPCSK9 (1 μg) digested without (lane 1) or with (lane 2) recombinat furin (0.5 μg) and cell lysate of rhΔ218PCSK9 (lanes 3 and 4) was subjected to SDS-PAGE followed by immunoblotting and detection with anti-Tetra-His antibody. (C) The reactivity of each monoclonal antibody (MAb) to purified rhPCSK9 (1.0 μg) was analyzed by 5–20% SDS-PAGE under nonreducing (lanes 1–5) and reducing (lanes 6–10) condition, followed by immunoblotting as described in the Materials and Methods. Lanes 1 and 6, monoclonal PCSK9 antibody (MAB38881; R&D Systems); lanes 2 and 7, Mab 1FB; lanes 3 and 8, Mab B12E; lanes 4 and 9, Mab B1G; lanes 5 and 10, Mab G12D. (D) The immunoprecipitation of human plasma with Mabs against PCSK9 was carried out. Immunoprecipitates were separated by a 5–20% SDS-PAGE under nonreducing condition, followed by immunoblotting and detection with monoclonal PCSK9 antibody (MAB38881). Lane 1, Mab 1FB; lane 2, Mab G12D; lane 3, Mab B1G; lane 4, Mab B12E. (E) The immunoprecipitation of human plasma with Mabs against PCSK9 was carried out. Immunoprecipitates were separated by a 5–20% SDS-PAGE under a nonreducing condition, followed by immunoblotting and detection with Mab G12D. Lane 1, Mab 1FB; lane 2, Mab G12D; lane 3, Mab B1G; lane 4, Mab B12E.

plasma TC, LDL-C, TG, ApoB, ApoC-II, ApoC-III, ApoE, and Lp(a), while the plasma levels of HDL-C, ApoA-I, and ApoA-II decreased by 13–16% (Table 1 and Supplemental Table 2). In FH heterozygotes, a similar reduction was shown.

Removal of PCSK9s in FH homozygotes or heterozygotes by LDL-A with DS columns

In FH homozygotes, the plasma levels of mature and furin-cleaved PCSK9 averaged 490 ± 173 ng/mL and 74 ± 23 ng/mL, respectively, before LDL-A treatment. The two forms of PCSK9 were, respectively, reduced by 56% and 55% in FH homozygotes by a single LDL-A procedure (Figure 2A). Furin-cleaved PCSK9 constituted approximately 15% of circulating PCSK9 in the plasma of FH patients. In FH heterozygotes, the plasma levels of the two forms of PCSK9 averaged 443 ± 128 ng/mL and 55 ± 26 ng/mL, respectively, before LDL-A treatment. The two forms of PCSK9 were reduced by 46% and 48% by a single LDL-A procedure in FH heterozygotes (Figure 2B). Thus, there were no significant differences in the reduction rate of either form of plasma PCSK9 after LDL-A between FH homozygotes and heterozygotes. In addition, plasma

levels of both PCSK9s in FH homozygotes before LDL-A treatment were not significantly different from those in the plasma of FH heterozygotes. As shown in Figure 3, there was a high degree of correlation between the reduction of plasma LDL-C and the reduction of mature PCSK9 in both FH homozygotes (r = 0.79; P = .036) and heterozygotes (r = 0.79; P = .004). In addition, there was a significant correlation between the reduction in plasma Lp(a) and that in mature PCSK9 in FH heterozygotes (r = 0.74; P = .0098; data not shown). On the other hand, there was no correlation between the reductions in plasma HDL-C and mature PCSK9 in FH homozygotes or heterozygotes (Supplemental Figure 4).

Crossover study of LDL-A treatment with DM columns in FH heterozygotes

A crossover study comparing the treatment efficacy between DS and DM columns was performed in 5 FH heterozygotes. A single LDL-A treatment with DM columns produced a 49–68% reduction in plasma TC, LDL-C, TG, ApoB, ApoC-II, ApoC-III, ApoE, and Lp(a), while the plasma levels of HDL-C, ApoA-I, and ApoA-II decreased by 23–26% (Supplemental Table 3). The plasma levels of mature and furin-cleaved PCSK9 before LDL-A treatment averaged 282 ± 36 ng/mL and 43 ± 28 ng/mL, respectively; the two forms were decreased by 56% and 48% by a single LDL-A treatment (Figure 2C).

Gel filtration chromatography of PCSK9 before and after a single LDL-A treatment

The plasma obtained before and after the single LDL-A treatment with DS columns was separated by gel filtration chromatography, and cholesterol and both forms of PCSK9 were measured in each fraction. Typical distribution patterns of cholesterol and PCSK9s are shown in Figure 4. Cholesterol levels were markedly reduced in the LDL fraction, while there was little change in the HDL fraction. Approximately 20% of mature PCSK9 coeluted with the apoB-containing fraction, and the rest coeluted with the apoB-deficient fraction. Meanwhile, in a portion of the FH patients, less than 5% of total PCSK9 was ob-

Table 1. Laboratory Data in FH Homozygotes and Heterozygotes Before and After a Single LDL-A Treatment With DS Columns

(mg/dL)	FH homozygotes (n = 7)			FH heterozygotes (n = 11)		
	Before	After	Reduction (%)	Before	After	Reduction (%)
TC	288 ± 63	86 ± 24[a]	70	220 ± 77	89 ± 41[a]	59
LDL-C	237 ± 49[d]	55 ± 22[a]	76	164 ± 75	51 ± 33[a]	69
HDL-C	31 ± 12	26 ± 9[a]	16	36 ± 18	32 ± 16	13
TG	99 ± 60	27 ± 21[a]	74	97 ± 43	30 ± 22[a]	70
Apo A-I	81 ± 22	71 ± 20[a]	13	99 ± 39	88 ± 35[a]	11
Apo A-II	22 ± 4	18 ± 4[a]	15	25 ± 8	21 ± 7[a]	14
Apo B	182 ± 44[d]	40 ± 21[a]	78	124 ± 46	36 ± 23[a]	71
Apo C-II	3.0 ± 2.3	1.3 ± 0.8[b]	54	3.6 ± 1.8	1.8 ± 1.3[a]	54
Apo C-III	8.5 ± 4.5	3.5 ± 1.6[a]	57	8.5 ± 2.8	4.6 ± 2.4[a]	48
Apo E	6.5 ± 2.1[c]	1.5 ± 0.8[a]	76	4.1 ± 0.8	1.1 ± 0.5[a]	73
Lp(a)	27 ± 22[d]	8.1 ± 5.8[b]	67	55 ± 27	19 ± 16[a]	68

Abbreviations: FH, familial hypercholesterolemia; HDL-C, high-density lipoprotein-cholesterol; LDL-C, low-density lipoprotein-cholesterol; Lp(a), lipoprotein (a); TC, total cholesterol; TG, triglyceride. All values are shown as mean ± SD.

n = 6 in Lp(a) of FH homozygotes.

[a] $P < 0.01$.

[b] $P < 0.05$ vs the respective values before LDL-A.

[c] $P < 0.01$.

[d] $P < 0.05$ vs the respective values in FH heterozygotes.

served in the apoB-fraction (data not shown). The distribution pattern of furin-cleaved PCSK9 was similar to that of mature PCSK9. Both forms of PCSK9s in the apoB-deficient fraction were reduced by 52–54%, while those in the apoB-containing fraction were reduced by 92–97%.

Coimmunoprecipitation of apoB in plasma of FH

To examine the association of apoB with PCSK9, plasma samples of FH were immunoprecipitated with monoclonal anti-apoB antibody. The control samples that were incubated in nonimmune serum instead of apoB antibody and negative control samples that were incubated in only resin showed no bands reactive to anti-apoB antibody (Figure 5A). Based on the coimmunoprecipitates of apoB, a mature PCSK9 band was detected by polyclonal PCSK9 antibody, confirming an association between mature PCSK9 and apoB in the plasma of FH. The band of furin-cleaved PCSK9 could not be detected in coimmuno-

precipitation of apoB, because it overlapped that of IgG (data not shown).

Profile of Lp(a) by gel filtration chromatography

To examine the association of Lp(a) with PCSK9 in the plasma of FH, Lp(a) was measured by ELISA in the collected fractions obtained by gel filtration analysis. Lp(a) was recovered predominantly in apoB-containing fraction, and was not recovered in the apoB-deficient fraction which contains the highest levels of both PCSK9s (Figure 5B).

Discussion

In the present study, we demonstrated that the two forms of plasma PCSK9 were removed by LDL-A treatment with either DS or DM columns in both FH homozygotes and heterozygotes based on measurements using a new sandwich ELISA. The two forms of PCSK9 were significantly decreased by 55–56% in FH homozygotes after a single LDL-A treatment with DS columns, and were decreased to a similar extent in FH heterozygotes after the treatment with DS or DM columns. The removal of two forms of PCSK9 would have contributed to some extent to the control of LDL-C medi-
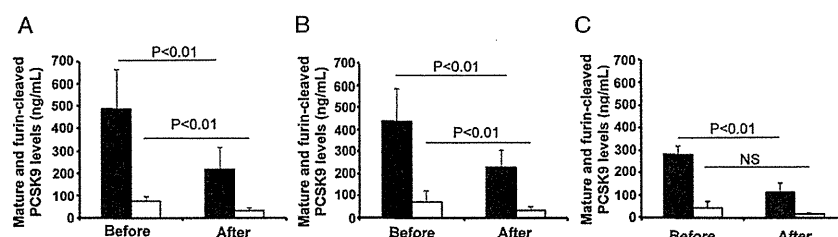

Figure 2. Change of plasma mature and furin-cleaved PCSK9 levels before and after a single LDL-A treatment. Plasma levels of mature (closed column) and furin-cleaved (open column) PCSK9s in (A) FH homozygotes (N = 7), (B) FH heterozygotes (N = 11) before and after LDL-A treatment with DS columns, and in (C) FH heterozygotes (N = 5) before and after LDL-A treatment with DM columns are shown.
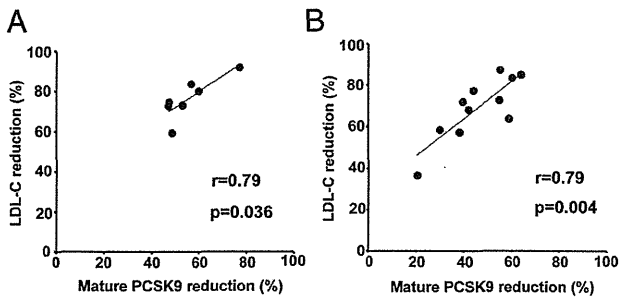
Figure 3. Correlation between plasma LDL-C reduction and mature PCSK9 reduction in FH homozygotes and FH heterozygotes. (A) Correlation between plasma LDL-C reduction (Y-axis) and mature PCSK9 reduction (X-axis) in FH homozygotes after a single LDL-A treatment with DS columns (N = 7). (B) Correlation between plasma LDL-C reduction (Y-axis) and mature PCSK9 reduction (X-axis) in FH heterozygotes after a single LDL-A treatment with DS columns (N = 11).

ated by LDLR in heterozygous FH or receptor-defective homozygous FH patients undergoing LDL-A treatment. However, it would not have contributed to the control of LDL-C in receptor-negative homozygous FH patients. In addition, DM columns whose treated volumes are limited are not usually used for patients who need a high volume of treated plasma. The use of DS columns is contraindicated for patients taking angiotensin-converting enzyme (ACE) inhibitors. Thus, we cannot decide whether DS or DM columns are superior, but we need to decide an appropriate application for each case.

Statins, the most effective commercially available medication for lowering serum LDL-C, decrease cholesterol synthesis, and increase LDLR activity in the liver. Meanwhile, they also stimulate expression of PCSK9, thereby reducing their own effects (23, 24). Thus, antisense oligonucleotides, RNA-mediated interference and Mabs that target PCSK9 have been developed as new treatment strategies for lowering LDL-C (25–29). The use of PCSK9-MAb could reduce the frequency of LDL-A and control LDL-C in heterozygous FH or homozygous FH patients with the LDLR defective type. In addition, the combination of PCSK-Mab and LDL-A treatment may improve the control of LDL-C synergistically or additively.

Recently, Dubic et al has developed an ELISA for the measurement of total PCSK9 using polyclonal antibodies (5). In the present study, we developed a new sandwich ELISA using Mabs for plasma mature and furin-cleaved PCSK9s, respectively, for the first time. This ELISA method could clarify association of the ratio of each form of PCSK9 with the effects of medication in hyperlipidemia patients with gain- or loss-of-function PCSK9 mutations and those taking cholesterol-lowering drugs (30), and with various conditions of hyperlipidemia concomitant with type II diabetes, obesity, and so on. In addition, it has been reported that furin-cleaved PCSK9 represents up to 40% of the total PCSK9 in normal subjects (9), whereas it
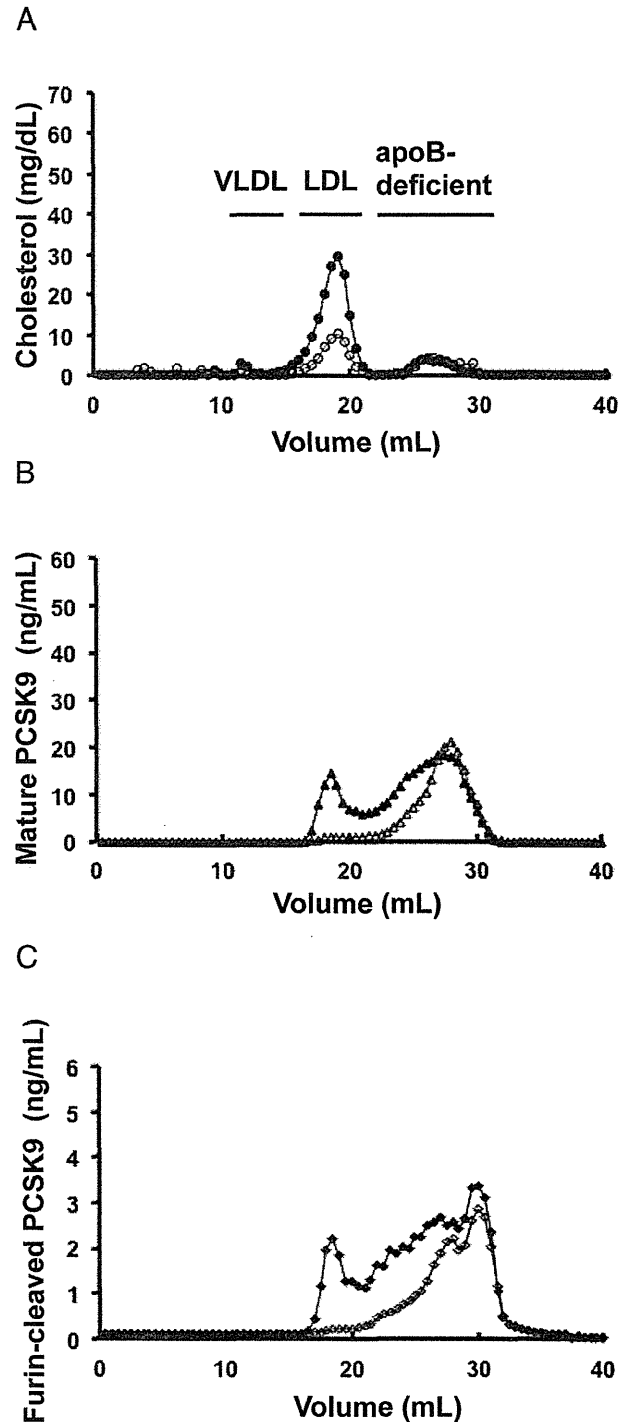

Figure 4. Typical gel filtration chromatography of mature and furin-cleaved PCSK9s and cholesterol in FH plasma before and after LDL-A treatment. Profiles of cholesterol (A, closed circles: before; open circles: after), mature (B, closed triangles: before; open triangles: after), and furin-cleaved PCSK9s (C, closed diamonds: before; open diamonds: after) were analyzed in FH plasma before and after a single LDL-A treatment with DS columns after fractionation by gel filtration chromatography as described in Materials and Methods.

represented 15% of the total PCSK9 in FH patients in the present study. We thus formed a hypothesis that FH shows high LDL-C levels due to not only LDLR mutations but also higher activity of LDLR degradation. The association
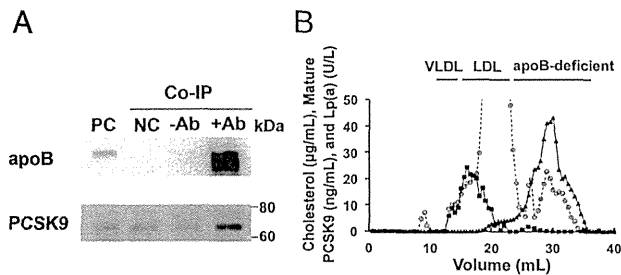
Figure 5. Coimmunoprecipitation of apoB and profile of Lp(a) by gel filtration chromatography in FH plasma. (A) Immunoprecipitation (IP) was performed with 500 µL of plasma from an FH patient treated by 1% triton X-100 and 0.5% sodium deoxycholate (final concentration). An equal volume of supernatants was also applied to columns without IgG and processed in the same way as the antibody coupling resin [negative control (NC)]. The immunoprecipitates were separated by 8–16% SDS-PAGE under denaturing and reducing conditions followed by immunoblotting with monoclonal anti-apoB antibody or polyclonal anti-PCSK9 antibody, and mouse TrueBlot® ULTRA: Anti-Mouse Ig HRP (eBioscience) or HRP-linked anti sheep IgG antibody (Santa Cruz Biotechnology Inc.). Control samples that were incubated in nonimmune serum were also analyzed (-Ab). The bands of apoB and PCSK9 were examined in an apoB-IP sample (+Ab). PC; positive control, -Ab; control-IP, +Ab; apoB-IP. (B) Profiles of Lp(a), cholesterol, and mature PCSK9 levels in the plasma from an FH patient as determined by gel filtration chromatography. Their levels in the collected fractions were measured as described in Materials and Methods. Closed squares: Lp(a); open circles: cholesterol; closed triangles: mature PCSK9 in plasma before LDL-A.

Recently, it has been reported that LDL-bound PCSK9 in human plasma exhibits diminished binding activity toward cell surface LDLR (31). However, it has not been clarified whether PCSK9-associated LDL is incorporated by LDLR, and further studies will be needed to examine the question. In addition, the interaction between apoB and PCSK9 has been reported to inhibit intracellular degradation of apoB and to result in increased secretion of apoB-containing lipoproteins (33). This secreted PCSK9-associated apoB may be derived from LDL associated with PCSK9 in plasma. A portion of PCSK9 may be bound to LDL extracellularly, thereby promoting cellular degradation of LDLR in the endosome.

In the present study, we found that the two forms of PCSK9 were reduced by 52–54% in the apoB-deficient fraction from gel filtration chromatography analysis. Circulating mature and furin-cleaved PCSK9s were mainly present in the apoB-deficient fraction. PCSK9s were removed by apoB-independent pathways based on the electric charge or nonspecific binding to the DS columns while they were removed based on particle size or nonspecific binding to the DM columns. The apoB-deficient fraction has been reported to contain PCSK9 that is mostly of a higher molecular weight, likely dimers and trimers (16, 32, 34). In addition, a previous study has shown that various proteins are present in this fraction, including albumin, globulin, serum amyloid-A, and more (35). LDL-A is thus suggested to remove circulating PCSK9 that is of high molecular weight, likely a dimmer or trimer, in association with these proteins in the apoB-deficient fraction. Meanwhile, other lipoproteins such as HDL have been reported to affect the self-association of PCSK9 (35). It has been calculated that two forms of PCSK9 are negatively charged (mature PCSK9: pI = 6.6; furin-cleaved PCSK9: pI = 7.02) (16), so they are not likely to bind directly to the DS column which is also negatively charged. A future study will be required to investigate the forms of PCSK9 in the apoB-deficient fraction.

The result that PCSK9 was removed by LDL-A in homozygous FH is not consistent with the report by Cameron et al (17). Because the columns used in their study were not described, they may have been different from those used in our present study or the study by Tavori et al (16). Thus, the differences in columns, race, life-style, forms of PCSK9 in plasma and proteins associated with PCSK9 may affect the removal of PCSK9 by LDL-A.

This study has some limitations. The major limitation is that a small sample size of 5 may be insufficient to test subtle differences between the two methods of apheresis on PCSK9. However, we could not get enough subjects for a crossover study comparing the treatment efficacy between DS and DM columns. A second limitation is that we

of the ratio of each form of PCSK9 with the regulation of LDL-C metabolism would be validated by the present method.

Gel filtration chromatography analysis showed that 20% of the total plasma PCSK9s existed in the apoB-containing fraction, which is a typical profile for plasma PCSK9 in FH patients (Figure 4). It has previously been reported that 35–39% or > 40% of PCSK9 was associated with the LDL fraction in normolipidemic subjects by size exclusion chromatography or natural density gradient (31, 32). Thus, it was suggested that the amount of PCSK9 contained in the apoB-containing fraction in the plasma of FH patients was lower than that in normolipidemic subjects. Two forms of PCSK9 were reduced by 92–97% in the LDL fraction on gel filtration chromatography and the reduction in mature PCSK9 was strongly correlated with that in LDL-C after a single LDL-A treatment (Figure 3). By immunoprecipitation, plasma mature PCSK9 was confirmed to be bound to apoB (Figure 5A). Thus, it was suggested that a portion of plasma PCSK9 was removed in association with apoB by LDL-A. The distribution of Lp(a) was not overlapped like that of mature PCSK9, suggesting that mature PCSK9 was not associated with Lp(a) (Figure 5B). In addition, the reason why PCSK9 associated with LDL decreases more than LDL-C has not been clarified. Further studies are necessary to clarify the mechanism underlying the removal of the proportion of PCSK9 associated with LDL by LDL-A.

did not perform a time-dependent study of rebound trajectories in LDL-C, apoB, Lp(a), and PCSK9 in the interval between apheresis. That could provide greater insight into the mechanisms of the coordinated regulation of apoB, Lp(a), and PCSK9. A third limitation is that the number of gel filtration analyses was limited because there were not enough plasma residues for analysis.

In conclusion, our present study has shown that plasma mature and furin-cleaved PCSK9s were removed in FH homozygotes and heterozygotes by binding to apoB or other mechanisms. This report is also the first to demonstrate for an ELISA method to measure both forms of plasma PCSK9—mature and furin-cleaved form—and this technique is expected to be useful for investigating the effects of medications or the physiological or pathological roles of PCSK9.

Acknowledgments

References

1. Goldstein JL, Hobbs HH, Brown MS. Familial hypercholesterolemia. In: Scriver CR BA, Sly WS, Valle D, eds. *The Metabolic and Molecular Bases of Inherited Disease.* 8th ed. New York: McGraw-Hill; 2001.
2. Abifadel M, Varret M, Rabès JP, et al. Mutations in PCSK9 cause autosomal dominant hypercholesterolemia. *Nature Genetics.* 2003; 34:154–156.
3. Benjannet S, Rhainds D, Essalmani R, et al. NARC-1/PCSK9 and its natural mutants: zymogen cleavage and effects on the low density lipoprotein (LDL) receptor and LDL cholesterol. *J Biol Chem.* 2004; 279:48865–48875.
4. Maxwell KN, Breslow JL. Adenoviral-mediated expression of Pcsk9 in mice results in a low-density lipoprotein receptor knockout phenotype. *Proc Natl Acad Sci USA.* 2004;101:7100–7105.
5. Dubuc G, Tremblay M, Paré G, et al. A new method for measurement of total plasma PCSK9: clinical applications. *J Lipid Res.* 2010; 51:140–149.
6. Alborn WE, Cao G, Careskey HE, et al. Serum proprotein convertase subtilisin kexin type 9 is correlated directly with serum LDL cholesterol. *Clin Chem.* 2007;53:1814–1819.
7. Benjannet S, Rhainds D, Hamelin J, Nassoury N, Seidah NG. The proprotein convertase (PC) PCSK9 is inactivated by furin and/or PC5/6A: functional consequences of natural mutations and post-translational modifications. *J Biol Chem.* 2006;281:30561–30572.
8. Essalmani R, Susan-Resiga D, Chamberland A, et al. In vivo evidence that furin from hepatocytes inactivates PCSK9. *J Biol Chem.* 2011;286:4257–4263.
9. Han B, Eacho PI, Knierman MD, et al. Isolation and characterization of the circulating truncated form of PCSK9. *J Lipid Res.* 2014; 55:1505–1514.
10. Lipari MT, Li W, Moran P, et al. Furin-cleaved proprotein convertase subtilisin/kexin type 9 (PCSK9) is active and modulates low density lipoprotein receptor and serum cholesterol levels. *J Biol Chem.* 2012;287:43482–43491.
11. Yokoyama S, Hayashi R, Satani M, Yamamoto A. Selective removal of low density lipoprotein by plasmapheresis in familial hypercholesterolemia. *Arteriosclerosis.* 1985;5:613–622.
12. Makino H, Harada-Shiba M. Long-term effect of low-density lipoprotein apheresis in patients with homozygous familial hypercholesterolemia. *Ther Apher Dial.* 2003;7:397–401.
13. Kobayashi J, Katsube S, Shimoda M, et al. Single LDL apheresis improves serum remnant-like particle-cholesterol, C-reactive protein, and malondialdehyde-modified-low-density lipoprotein concentrations in Japanese hypercholesterolemic subjects. *Clin Chim Acta.* 2002;321:107–112.
14. Kojima S, Harada-Shiba M, Toyota Y, et al. Changes in coagulation factors by passage through a dextran sulfate cellulose column during low-density lipoprotein apheresis. *Int J Artif Organs.* 1992;15:185–190.
15. Yuasa Y, Osaki T, Makino H, et al. Proteomic analysis of proteins eliminated by low-density lipoprotein apheresis. *Ther Apher Dial.* 2014;18:93–102.
16. Tavori H, Giunzioni I, Linton MF, Fazio S. Loss of plasma proprotein convertase subtilisin/kexin 9 (PCSK9) after lipoprotein apheresis. *Circ Res.* 2013;113:1290–1295.
17. Cameron J, Bogsrud MP, Tveten K, et al. Serum levels of proprotein convertase subtilisin/kexin type 9 in subjects with familial hypercholesterolemia indicate that proprotein convertase subtilisin/kexin type 9 is cleared from plasma by low-density lipoprotein receptor-independent pathways. *Transl Res.* 2012;160:125–130.
18. Mabuchi H, Miyamoto S, Ueda K, et al. Causes of death in patients with familial hypercholesterolemia. *Atherosclerosis.* 1986;61:1–6.
19. Harada-Shiba M, Arai H, Oikawa S, et al. Guidelines for the management of familial hypercholesterolemia. *J Atheroscler Thromb.* 2012;19:1043–1060.
20. Harada-Shiba M, Takagi A, Miyamoto Y, et al. Clinical features and genetic analysis of autosomal recessive hypercholesterolemia. *J Clin Endocrinol Metab.* 2003;88:2541–2547.
21. Ishihara M, Kujiraoka T, Iwasaki T, et al. A sandwich enzyme-linked immunosorbent assay for human plasma apolipoprotein A-V concentration. *J Lipid Res.* 2005;46:2015–2022.
22. Oka T, Kujiraoka T, Ito M, et al. Distribution of phospholipid transfer protein in human plasma: presence of two forms of phospholipid transfer protein, one catalytically active and the other inactive. *J Lipid Res.* 2000;41:1651–1657.
23. Dubuc G, Chamberland A, Wassef H, et al. Statins upregulate PCSK9, the gene encoding the proprotein convertase neural apop-

tosis-regulated convertase-1 implicated in familial hypercholester-olemia. *Arterioscler Thromb Vasc Biol.* 2004;24:1454–1459.

24. Dong B, Wu M, Li H, et al. Strong induction of PCSK9 gene expression through HNF1alpha and SREBP2: mechanism for the resistance to LDL-cholesterol lowering effect of statins in dyslipidemic hamsters. *J Lipid Res.* 2010;51:1486–1495.

25. Frank-Kamenetsky M, Grefhorst A, Anderson NN, et al. Therapeutic RNAi targeting PCSK9 acutely lowers plasma cholesterol in rodents and LDL cholesterol in nonhuman primates. *Proc Natl Acad Sci USA.* 2008;105:11915–11920.

26. Yamamoto T, Harada-Shiba M, Nakatani M, et al. Cholesterol-lowering action of BNA-based antisense oligonucleotides targeting PCSK9 in atherogenic diet-induced hypercholesterolemic mice. *Mol Therapy Nucleic Acids.* 2012;1:e22.

27. Chan JC, Piper DE, Cao Q, et al. A proprotein convertase subtilisin/kexin type 9 neutralizing antibody reduces serum cholesterol in mice and nonhuman primates. *Proc Natl Acad Sci USA.* 2009;106:9820–9825.

28. Stein EA, Gipe D, Bergeron J, et al. Effect of a monoclonal antibody to PCSK9, REGN727/SAR236553, to reduce low-density lipoprotein cholesterol in patients with heterozygous familial hypercholesterolaemia on stable statin dose with or without ezetimibe therapy: a phase 2 randomised controlled trial. *Lancet.* 2012;380:29–36.

29. Giugliano RP, Desai NR, Kohli P, et al. Efficacy, safety, and tolerability of a monoclonal antibody to proprotein convertase subtilisin/kexin type 9 in combination with a statin in patients with hyper-cholesterolaemia (LAPLACE-TIMI 57): a randomised, placebo-controlled, dose-ranging, phase 2 study. *Lancet.* 2012;380:2007–2017.

30. Nozue T, Hattori H, Ishihara M, et al. Comparison of effects of pitavastatin versus pravastatin on serum proprotein convertase subtilisin/kexin type 9 levels in statin-naïve patients with coronary artery disease. *Am J Cardiol.* 2013;111:1415–1419.

31. Kosenko T, Golder M, Leblond G, Weng W, Lagace TA. Low density lipoprotein binds to proprotein convertase subtilisin/kexin type-9 (PCSK9) in human plasma and inhibits PCSK9-mediated low density lipoprotein receptor degradation. *J Biol Chem.* 2013;288: 8279–8288.

32. Tavori H, Fan D, Blakemore JL, et al. Serum proprotein convertase subtilisin/kexin type 9 and cell surface low-density lipoprotein receptor: evidence for a reciprocal regulation. *Circulation.* 2013;127: 2403–2413.

33. Sun H, Samarghandi A, Zhang N, Yao Z, Xiong M, Teng BB. Proprotein convertase subtilisin/kexin type 9 interacts with apolipoprotein B and prevents its intracellular degradation, irrespective of the low-density lipoprotein receptor. *Arterioscler Thromb Vasc Biol.* 2012;32:1585–1595.

34. Fan D, Yancey PG, Qiu S, et al. Self-association of human PCSK9 correlates with its LDLR-degrading activity. *Biochemistry.* 2008; 47:1631–1639.

35. Holzer M, Trieb M, Konya V, Wadsack C, Heinemann A, Marsche G. Aging affects high-density lipoprotein composition and function. *Biochim Biophys Acta.* 2013;1831:1442–1448.

Brief Communication

Evaluation of Multiple-Turnover Capability of Locked Nucleic Acid Antisense Oligonucleotides in Cell-Free RNase H-Mediated Antisense Reaction and in Mice

Tsuyoshi Yamamoto,[1] Naoko Fujii,[1] Hidenori Yasuhara,[1] Shunsuke Wada,[1] Fumito Wada,[1]
Naoya Shigesada,[1] Mariko Harada-Shiba,[2] and Satoshi Obika[1]

The multiple-turnover ability of a series of locked nucleic acid (LNA)-based antisense oligonucleotides (AONs) in the RNase H-mediated scission reaction was estimated using a newly developed cell-free reaction system. We determined the initial reaction rates of AONs under multiple-turnover conditions and found that among 24 AONs tested, AONs with melting temperatures (*T*m) of 40°C–60°C efficiently elicit multiple rounds of RNA scission. On the other hand, by measuring *T*m with two 10-mer RNAs partially complementary to AONs as models of cleaved 5′ and 3′ fragments of mRNA, we found that AONs require adequate binding affinity for efficient turnover activities. We further demonstrated that the efficacy of a set of 13-mer AONs in mice correlated with their turnover efficiency, indicating that the intracellular situation where AONs function is similar to multiple-turnover conditions. Our methodology and findings may provide an opportunity to shed light on a previously unknown antisense mechanism, leading to further improvement of the activity and safety profiles of AONs.

Introduction

A NTISENSE OLIGONUCLEOTIDES (AONs) having specific configurations compatible with RNase H-inducible capacity have been developed over decades and have been shown to be very powerful and robust gene silencing materials in cultured cells and animals, as well as in humans (Crooke, 2007; Yamamoto et al., 2011). In particular, the "gapmer" configuration, which is a chimeric AON consisting of a central RNase H-recruitable DNA stretch pinched by affinity-enhancing modified nucleic acids with fully phosphorothioated (PS) internucleotide linkages, has shown great promise. Affinity-enhancing modified nucleic acids, such as MOE (2′-O-methoxyethyl RNA), 2′,4′-BNA/LNA (2′-O,4′-C-methylene bridged nucleic acid/locked nucleic acid) (Fig. 1A) (Obika et al., 1997; Obika et al., 1998; Singh et al., 1998), and other bridged nucleic acids (BNAs) (Hari et al., 2006; Miyashita et al., 2007; Seth et al., 2009; Prakash et al., 2010; Yahara et al., 2012) mostly interfere with RNase H activity, but when used in a chimeric gapmer, they assist in enhancing target binding and nuclease stability, greatly improving its potency without affecting RNase H capacity. Despite these innovations, very few products have been released on the market and some candidates in clinical trials have been dropped due to efficacy and safety issues.

More recently, Straarup et al. successfully improved efficacy of an earlier LNA-based gapmer targeting apolipopro- tein B-100 (apoB) by trimming its conventional long-strand [16~20 nucleotides (nt)] and utilizing the resulting shorter LNA gapmers (~13 nt) (Straarup et al., 2010). Our group also independently reproduced and extended this observation by using newly developed 2′,4′-BNA^{NC} chemistry and supported the unusual notion that a drug with weaker binding has stronger silencing activity (Fig. 1A) (Yamamoto et al., 2012b). One possible explanation for this finding is that shorter AONs accelerate the reaction to a greater degree than conventional AONs *via* turnover mechanisms. Stanton et al. recently observed that melting temperatures (*T*m) of greater than 80°C showed reduced silencing activity and explained this finding as a result of an inability to recycle AONs in cells (Stanton et al., 2012). However, to the best of our knowledge, there is no experimental evidence of AON turnover, despite its anticipated importance as in RNAi mechanisms (Hutvagner and Zamore, 2002). If turnover of AONs was demonstrated in antisense mechanisms, a more favorable configuration or chemistry that accelerates AON turnover may be discovered, and this discovery could lead to additional insights into strategies for further improving the activity and safety of AONs. Most previous works related to antisense reaction kinetics have been conducted to determine whether duplexes of interest have an ability to elicit RNase H, and are thus performed under excess amounts of AON/RNA duplex over RNase H in cell-free systems (single-turnover conditions for AON) (Crooke et al., 1995; Lima and Crooke,

[1]Graduate School of Pharmaceutical Sciences, Osaka University, Suita, Osaka, Japan.
[2]Department of Molecular Innovation in Lipidology, National Cerebral and Cardiovascular Center Research Institute, Suita, Osaka, Japan.
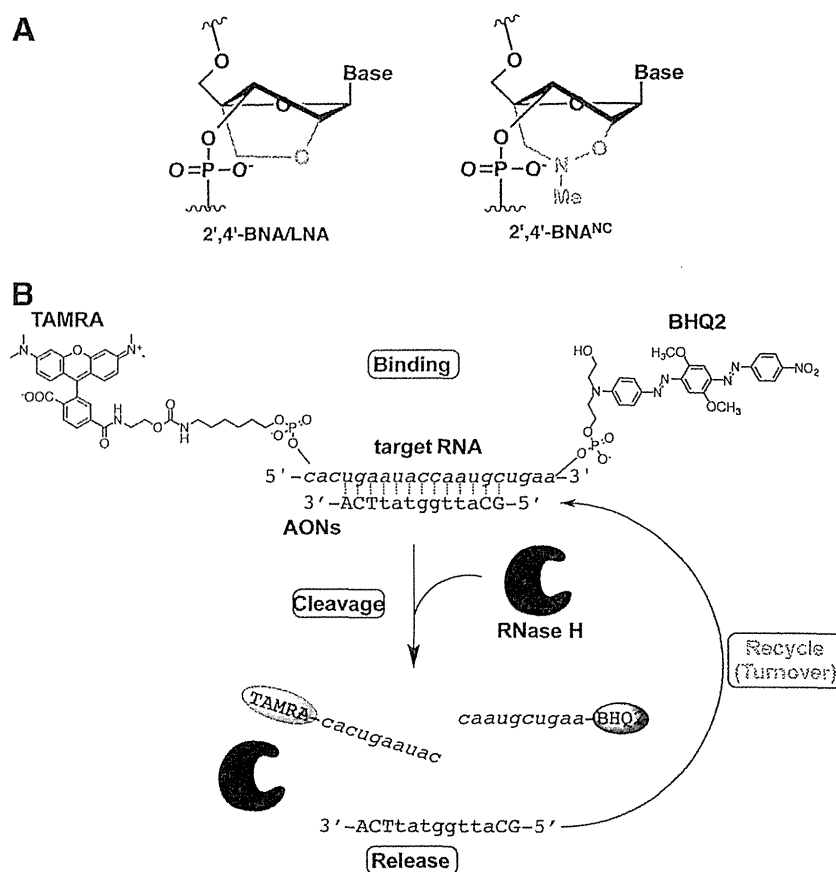
A

2',4'-BNA/LNA   2',4'-BNA^NC

B

FIG. 1. Recycling of antisense oligo-nucleotides in antisense reaction. (**A**) Structures of bridged nucleic acids (BNAs). (**B**) Schematic illustration of cell-free Förster resonance energy transfer (FRET)-based turnover monitoring system used in this study. Color images available online at www.liebertpub.com/nat

1997; Vester et al., 2008; Stanton et al., 2012). In the present study, to investigate whether AONs are recyclable in antisense reactions, we devised a cell-free reaction system, in which synthetic 20-mer target RNA conjugated with a pair of FRET (Förster resonance energy transfer) dyes and *Escherichia coli*–derived RNase H are both in excess over AONs (multiple-turnover conditions). In this system, an increase in fluorescence from the FRET donor is observed after binding, cleavage, and release proceeds sequentially (Fig. 1B). The main problem facing previous works is the potential difficulty in separating affinity issues from length issues, because affinity usually varies as a function of strand length. In this study, we utilized LNA, which enables us to freely modify AON affinity without changing length; thus, we prepared a series of LNA-based apoB-targeting AONs with a central focus on 13-mer AONs (Table 1), one of which (ApoB-13a) had been previously characterized as highly potent *in vitro* and *in vivo* (Straarup et al., 2010; Yamamoto et al., 2012b).

Materials and Methods

Oligonucleotides

All oligonucleotides listed in Table 1 were purchased from Gene Design Inc.

Thermal denaturation experiments

Thermal denaturation experiments were carried out on SHIMADZU UV-1650 and UV-1800 spectrometers equip-

ped with a Tm analysis accessory. For duplex formation, equimolecular amounts of target RNA and each AON were dissolved in 10 mM sodium phosphate buffer (pH = 7.2) containing 100 mM (1.0 M for MRNA-1, MRNA-2) NaCl to give a final strand concentration of 2.0 μM. Duplex samples were then annealed by heating at 90°C, followed by slow cooling to room temperature. Melting profiles were recorded at 260 nm from 0°C to 95°C at a scan rate of 0.5°C/minute. Melting temperatures were obtained as maxima of the first derivative of the melting curves.

Turnover experiments

Dual-labeled complementary RNA probe (DL-MRNA) and non-labeled complementary 20-mer RNA (NL-MRNA) were combined in a 1:3 molar ratio. The intended amounts of the resulting mixture and AON were added to RNase H reaction buffer (New England Biolabs). The reaction was initiated by addition of 1 μL of the intended concentrations of *E. coli* RNase H (Takara) to 199 μL of reaction mixture. Fluorescence intensity was recorded once every 15 seconds for 15 minutes at 555 nm (ex) and 590 nm (em) using a fluorescence microplate reader (Molecular Devices). The initial turnover rates ($v0$) were calculated by fitting a linear regression line to the data for the first 0–60 seconds and then converted the resulting slopes expressed as RFU/second into $v0$ (nM/second) by using a conversion factor, 6.15 (RFU/nM), determined by experiments shown in Supplementary Fig. S1 (Supplementary Data are available online at www .liebertpub.com/nat).

TABLE 1. OLIGONUCLEOTIDES USED IN THIS STUDY

No.	Sequence ID	Sequence	T_m (°C)
1	ApoB-20a	5′-TTCAGcattggtattCAGTG-3′	76±0.4
2	ApoB-20b	5′-T°T°C°A°GcattggtattC°A°G°T°G-3′	79±0.6
3	ApoB-20c	5′-t°t°c°a°g°c°a°t°t°g°g°t°a°t°t°c°a°g°t°g-3′	59±0.6
4	ApoB-16a	5′-CAGcattggtatTCAG-3′	66±0.5
5	ApoB-14a	5′-AGCattggtatTCA-3′	62±0.6
6	ApoB-14b	5′-AgCattggtatTcA-3′	58±0.4
7	ApoB-13a	5′-GCattggtatTCA-3′	59±0.5
8	ApoB-13b	5′-G°CattggtatT°C°A-3′	62±0.1
9	ApoB-13c	5′-gCattGgtatTCA-3′	63±0.5
10	ApoB-13d	5′-GcattggtaTTCA-3′	58±0.8
11	ApoB-13e	5′-GCattggtattCA-3′	55±0.5
12	ApoB-13f	5′-G°CattggtattC°A-3′	57±0.1
13	ApoB-13g	5′-GCattggtatTcA-3′	58±0.6
14	ApoB-13h	5′-gcattggtatTCA-3′	48±0.7
15	ApoB-13i	5′-GCAttggtattca-3′	50±0.5
16	ApoB-12a	5′-GCattggtatTC-3′	52±0.6
17	ApoB-12b	5′-GCattggtaTtC-3′	53±0.5
18	ApoB-12c	5′-G°CattggtatT°C-3′	54±0.5
19	ApoB-11a	5′-CAttggtatTC-3′	39±0.5
20	ApoB-11b	5′-C°AttggtatT°C-3′	41±0.4
21	ApoB-10a	5′-CattggtatT-3′	28±0.4
22	ApoB-10b	5′-CAttggtaTT-3′	33±0.6
23	ApoB-10c	5′-C°AttggtaT°T-3′	36±0.5
24	ApoB-10d	5′-cattggtATT-3′	29±0.5
25	DL-MRNA	5′-R-cacugaauaccaaugcugaa-Q-3′	
26	NL-MRNA	5′-cacugaauaccaaugcugaa-3′	
27	MRNA-1	5′-cacugaauac-3′	
28	MRNA-2	5′-caaugcugaa-3′	

Upper case, lower case, lower italic, and superscript circle indicate locked nucleic acid (LNA), DNA, RNA, and phosphodiester linkage, respectively. All internucleotide linkages are phosphorothioated unless otherwise noted. All RNAs numbered 25, 26, 27, and 28 have phosphodiester internucleotide linkages. Melting temperatures (T_m) are shown as mean±SD.

apoB, apolipoprotein B-100; dl-mrna, dual-labeled complementary RNA probe; nl-mrna, non-labeled complementary 20-mer RNA.

In vivo pharmacological experiments

All animal procedures were performed in accordance with the guidelines of the Animal Care Ethics Committee of the National Cerebral and Cardiovascular Center Research Institute. All animal studies were approved by an institutional review board. All C57BL/6J mice (CLEA Japan) were male, and studies were initiated when animals were 8 weeks of age. Mice were maintained on a 12-hour light/12-hour dark cycle and fed ad libitum. Mice received a single treatment of AONs administered subcutaneously at a dose of 0.75 mg/kg. At the time of sacrifice, mice were anesthetized and livers were harvested and snap frozen until subsequent analysis. Whole blood was collected and subjected to serum separation for subsequent analysis.

mRNA quantification

Total RNA was isolated from mouse liver tissues using TRIzol Reagent (Life Technologies Japan) in accordance with the manufacturer's instructions. Gene expression was evaluated using a two-step quantitative reverse transcription-polymerase chain reaction (RT-PCR) method. Reverse transcription of RNA samples was performed using a High-Capacity cDNA Reverse-Transcription Kit (Life Technologies), and quantitative PCR was performed using TaqMan Gene Expression Assays (Life Technologies Japan). Messenger RNA levels of apoB were normalized against GAPDH mRNA levels. For murine apoB and GAPDH, TaqMan gene expression assays were used (assay IDs: Mm01545156_m1 and Mm99999915_g1, respectively).

AON quantification in liver

Assay was performed as described previously (Yamamoto et al., 2012a). Template DNA: 5′-gaatagcgatgaataccaatgc-3′ with biotin at the 3′ end; ligation probe DNA: 5′-tcgctattc-3′ with phosphate at the 5′ end and digoxigenin at the 3′ end.

Serum chemistry

Assay kits (#439-17501; WAKO) were used to measure serum levels of total cholesterol.

Statistics

Pharmacological studies were performed with more than three mice per treatment group. All data are expressed as means±standard deviation (SD). $P < 0.05$ was considered to be statistically significant in all cases. Statistical comparisons were performed by Dunnett's or Bonferroni's multiple comparison tests.

Results and Discussion

Our first goal was to prepare bioactive AONs with a variety of binding affinities for the target RNA. We designed and

synthesized 24 AONs, as shown in Table 1. Most of the AONs were 10- to 20-mer LNA/DNA chimeras with full or partial PS backbones. DNA stretches on these AONs were kept in the 6- to 10-nt range, which is expected to be sufficient for eliciting RNase H of both *E. coli* and mammalian origins (Monia et al., 1993; Kurreck et al., 2002). ApoB-13c containing LNA in the center of the gap was prepared as a non-cleavable negative control. We next determined *T*m values of all AONs with the NL-MRNA (Table 1). As expected, *T*m values of these AONs were uniformly and broadly distributed from approximately 30° to 80°C under the indicated buffer conditions.

In order to investigate turnover activities of AONs, we developed a cell-free fluorescent turn-on system. DL-MRNA labeled with reporter dye (TAMRA) and quencher (BHQ2) on the 5′ and 3′ termini, respectively, was designed and prepared to detect RNA scission. Using this probe, we first evaluated the turnover activity of previously validated ApoB-13a. In the presence of an 80- to 240-fold molar excess of complementary RNA, 10 nM ApoB-13a was pre-incubated at 37°C in a 96-well microplate before addition of RNase H. It should be noted that the target complementary RNA used here consists of one-quarter dual-labeled DL-MRNA and three-quarters non-labeled NL-MRNA to avoid undesirable quenching or other interactions that may affect fluorescence (Supplementary Table S1). After addition of 60 units per well RNase H to the reactions, fluorescence intensities of TAMRA were measured (excitation = 555 nm and emission = 590 nm) every 15 seconds for 15 minutes (Supplementary Fig. S1A). Fluorescence of the reporter dye increased over time. The initial reaction rates also increased as a function of RNA concentration, where the initial reaction rates were determined from the slope of the initial linear portions (0–60 seconds) of the plots of fluorescence intensity versus time. In contrast, time-dependent fluorescence changes in TAMRA were not seen in an ApoB-13a-lacking control. We also observed very low background fluorescence levels in the control group, which indicates efficient quenching of TAMRA fluorescence by BHQ2, despite these dyes being 20 nt distant from one another. The fluorescence increases reached a plateau at 5 minutes. We confirmed that this indicates the completion of degradation of all target RNAs and then attempted to estimate the conversion coefficient between fluorescence intensity and concentration of RNA (Supplementary Figs. S1B, S2). By plotting fluorescence intensities at 15 minutes as a function of RNA concentration, we found high linear correlations between fluorescence intensity and concentration and determined 6.15 (RFU/nM) as a conversion factor. To determine the required amount of RNase H in this system, we performed further tests with various amounts of RNase H (2–180 units/well). A near maximum reaction rate could be obtained when at least 60 units/well of RNase H were added to the reaction, and confirmed that the rate-determining step of this reaction was not the scission step, but was the recycling step under these conditions (Supplementary Fig. S3). Taken together, these results are consistent with the recycling of ApoB-13a during this cell-free antisense reaction (see also Supplementary Fig. S4; Supplementary Table S2), and this system is useful for rapid screening of multiple-turnover activities of a series AONs.

We next aimed to measure a set of initial rates of AONs (Table 1). The initial velocities were determined as described

above. At a concentration of 10 nM, each AON was incubated in the presence of 800 nM complementary RNA (DL-MRNA:NL-MRNA = 1:3) and 60 units/well RNase H. Time-dependent fluorescence changes were measured and initial rates were subsequently determined. The observed initial rates were rearranged in ascending order of *T*m values of corresponding AONs and are shown in Fig. 2A. As expected, we found an inverted U-shaped relationship between initial rate and *T*m values on the whole: AONs with high (> 60°C) and low (< 30°C) *T*m values have relatively small initial rates, while AONs having *T*m of 40°C–60°C showed efficient turnover in this system. This implies that AONs having higher multiple-turnover activities are more potent than conventional long LNA gapmers with extraordinarily high affinity. On the other hand, ApoB-12a showed the highest turnover ability among AONs tested, but ApoB-12a was shown to be less potent than ApoB-13a *in vivo* (Straarup et al., 2010). Thus, interpreting these data, we must take into account the differences between experimental buffer conditions used here and physiological conditions. For instance, it is known that longer PS-DNAs are more likely to form stronger undesirable complexes with proteins and inactivate RNase H to reduce their efficacy (Gao et al., 1992; Watanabe et al., 2006). As in this system, there are limited accompanying components such as inorganics, proteins, and lipids, and effects including such length-dependent factors may not have been considered. Among the four 10-mer LNAs, ApoB-10a and ApoB-10d showed marked inefficient turnover activity when compared with ApoB-10b and ApoB-10c, indicating a lack of binding affinity. In contrast, the two 20-mer AONs showed inefficient turnover activities when compared with ApoB-20c, probably due to slow product release.

Surprisingly, turnover activities of ApoB-13d and ApoB-13h were exceptionally low, although their *T*m values were in an active range (Fig. 2A). To better understand this observation, we further measured *T*m values of AONs with two additional 10-mer RNAs (MRNA-1, MRNA-2) (Fig. 2B). MRNA-1 and MRNA-2 were prepared as models for the cleaved products of RNase H and correspond to the 5′ and 3′ halves of NL-MRNA, respectively. The results showed that melting temperatures for MRNA-1 were lower than those for MRNA-2, but this trend was reversed in ApoB-13d and ApoB-13h. This potential affinity bias may explain the difference in efficiency of turnover activity. The consensus sequence for the preferred RNase H cleavage sites is unknown; instead, a strong positional preference for cleavage has been observed in a family of enzymes. For example, human RNase H1 has been shown to preferentially cleave the RNA part of RNA/DNA hybrid several nucleotides away from the 5′-RNA/3′-DNA terminus, probably due to the binding directionality of the enzyme (Lima et al., 2007a; Lima et al., 2007b). It has been predicted that the hybrid binding domain of RNase H binds the 5′-RNA/3′-DNA flank of the hybrid relative to the catalytic domain, which is strongly supported by the crystal structure of human RNase H with RNA/DNA hybrids (Nowotny et al., 2007). Despite some reported differences between *E. coli* and human RNase H such as a minimal gap size required for activation of RNase H (Monia et al., 1993; Crooke et al., 1995), the high similarity of the structures of human RNase H1 and *E. coli* RNase H1 suggests that this positional directionality for cleavage encourages ApoB-13d to produce longer RNA segments than fragments
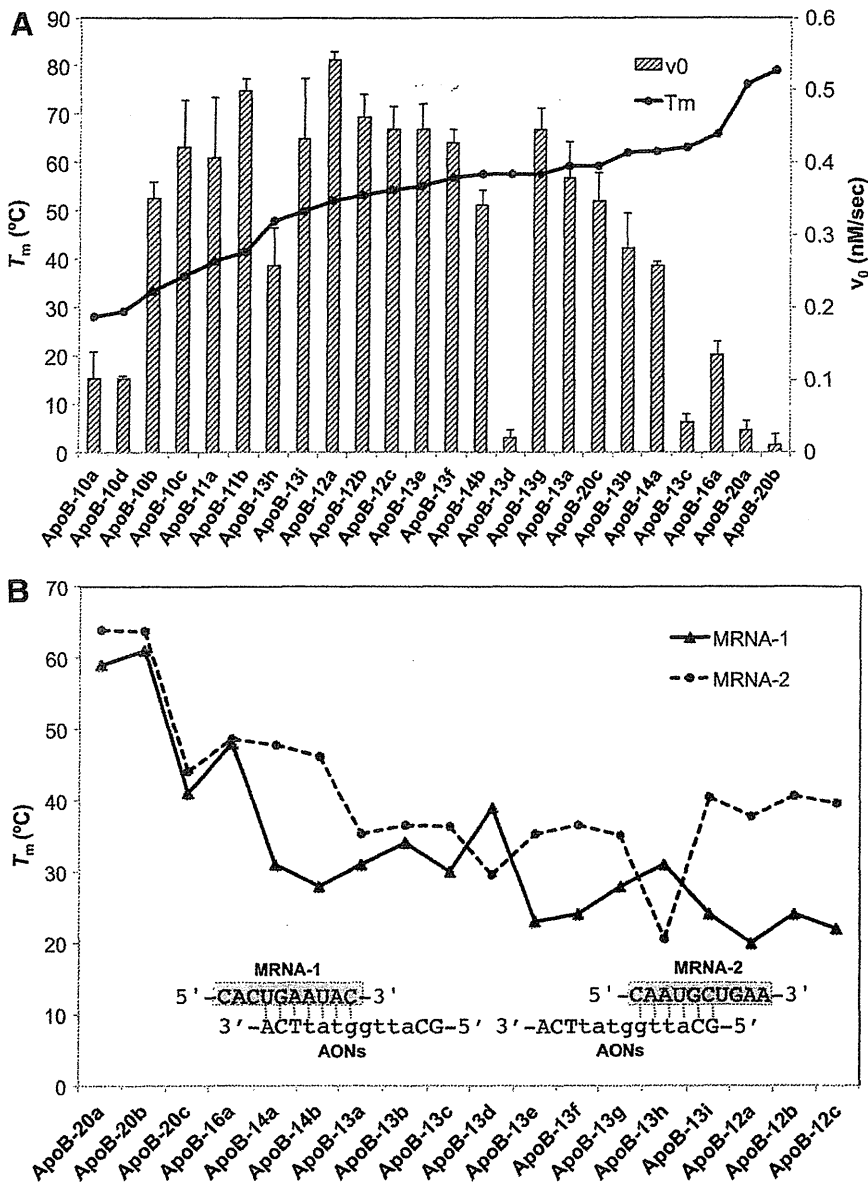
FIG. 2. (A) Relationship between turnover rate and gross or local affinity. Initial rates (v_0, bar graph) of turnover reaction rearranged in ascending order of melting temperature (T_m) values (*black line*) of corresponding antisense oligonucleotides (AONs). Data are means ± standard deviation (SD). (B) Melting temperatures with MRNA-1 (*solid*) and MRNA-2 (*dotted*). All experiments here were repeated at least three times. Color images available online at www.liebertpub.com/nat

produced by other AONs, thereby forming very stable duplexes with the 3′ half of ApoB-13d and eventually decelerating product release, as well as turnover. Collectively, the requirements for high turnover rates would be adequate binding affinity of the duplex formed by using several bases of AON (for the rapid release of cleaved mRNA), as well as moderate binding affinity of full-length AON/mRNA duplex (for efficient target capture). In contrast, the affinity of the 5′ half of ApoB-13h is thought to be too low to form stable duplexes for cleavage.

In order to explore the capacity of turnover under biological conditions, we attempted to evaluate the *in vivo* efficacy of AONs with identical length (ApoB-13a, -13d, -13e, -13g, and -13h), and to compare the *T*m data relevant to turnover activity. We here adopted a low dosage of 0.75 mg kg⁻¹, which had been confirmed as being sufficient to achieve knockdown of the target apoB mRNA for ApoB-13a, a positive control for *in vivo* screening, because even a single administration of a relatively low dose of 5 mg/kg ApoB-13a had

been shown to reduce apoB mRNA by 97%, which made it difficult to discriminate differences in efficacy when AONs screened have similar high efficacy (Straarup et al., 2010). Mice (n = 3/group) were dosed subcutaneously with 0.75 mg kg⁻¹ ApoB-13a, -13d, -13e, -13g and -13h. After 48 hours post-injection, expression levels of apoB mRNA in the liver were analyzed. The apoB mRNA reduction is associated with the clinically relevant therapeutic phenotype characterized by reduced blood cholesterol concentration for the treatment of hypercholesterolemia. Expression levels were rearranged in ascending order of *T*m values of corresponding AONs vs full-length NL-MRNA and are described in Fig. 3. The highest level of reduction in hepatic apoB mRNA was observed in ApoB-13a, while the lowest level of reduction was observed in ApoB-13d and -13h (Fig. 3A; Supplementary Table S3). Statistical significance was seen for ApoB-13a, -13e and -13g, but not for ApoB-13d and -13h. A similar-sized LNA phosphorothioate oligonulecotide without target sites on apoB mRNA was used as a control, showing no decrease in

FIG. 3. Reduction of apoB mRNA in the livers (bar graph) of mice ($n = 3$/group) receiving a single subcutaneous dose of 0.75 mg kg^{-1} of a series of 13-mer AONs (**A**) rearranged in ascending order of T_m values along with melting temperatures versus MRNA-1 (*solid*) and MRNA-2 (*dashed*). Dunnett's multiple comparison test, ***$p < 0.001$; **$p < 0.01$; N.S., not significant. (**B**) The mouse liver content of a series of 13-mer AONs. Bonferroni multiple comparison tests did not reveal any of arms to be significantly different across groups, $p < 0.05$. Error bars represent group means + SD $n = 3$.
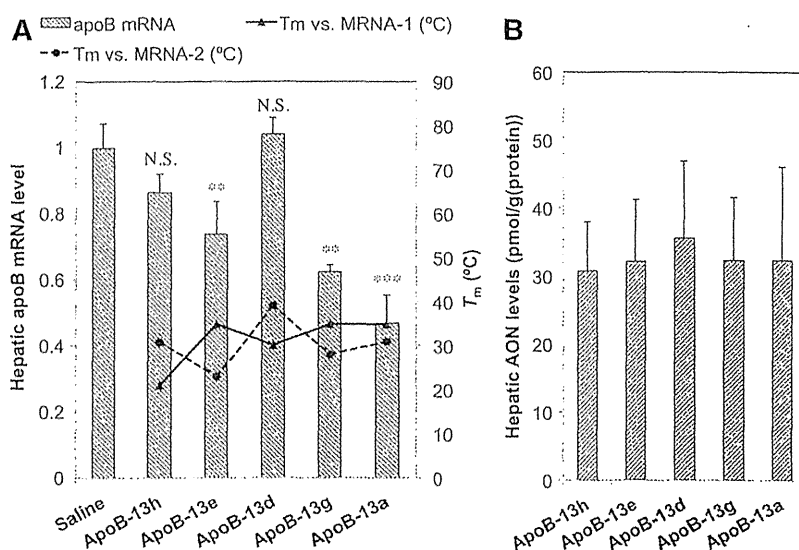
hepatic apoB mRNA and no potential toxicity (Supplementary Tables S3, S4).

The efficacy order of ApoB-13a > - 13g > - 13e > - 13h > - 13d appears to be unrelated to binding affinity to full-length NL-MRNA, but inefficiency of ApoB-13d and ApoB-13h *in vivo* were consistent with their slow turnover rates in the cell-free system, while other AONs are potent *in vivo* and show fast turnover rates in the cell-free system. Serum reduction levels in total cholesterol denoted the same tendency as mRNA reduction levels (Supplementary Fig. S5). As we selected AONs with an identical length of 13 nt, identical sequences and similar compositions for *in vivo* examination, the mouse liver content of these 13-mer AONs was measured and found to be almost identical (Fig. 3B). In addition to this, we speculate that AONs are not necessarily in vast excess of mRNA even *in vivo*. Sohlenius-Sternbeck has estimated a hepatocellularity number for humans, mice and other animal livers (Sohlenius-Sternbeck, 2006). The value for mice was estimated to be 135×10^6 cells per gram of liver, where livers of 8-week-old mice are 1.0 gram on average. On the other hand, we and others have calculated that approximately <10% of dosed oligonucleotides (<400 pmol for 0.75 mg/kg) reside in liver, even at 48–72 h post-dosing (Straarup et al., 2010; Yamamoto et al., 2012a).

Considering these conditions, each parenchymal cell may be exposed to AONs to a lesser extent than it is in a conventional *in vitro* transfection experiment. Furthermore, nonparenchymal cells such as Kupffer cells are thought to be more likely to ingest AONs than apoB-expressing parenchymal cells do and intracellular distribution of AONs *via* non-productive uptake further reduces the active form of AONs (Koller et al., 2011). In the light of this context, our *in vivo* multiple-turnover hypothesis is a compelling explanation for the *in vivo* activity of AONs. Of course, as there may exist differences such as intracellular distribution of AONs into productive versus less productive compartments, which can be influenced by small changes in chemistry and protein binding ability, it is necessary to continue gathering evidence. This hypothesis may also offer a new direction with

regard to the remaining issues in antisense drug development; for example, inconsistency between *in vitro* gene silencing activity of AONs delivered in complex with transfection vehicles and *in vivo* activity of naked AONs (Stein et al., 2010; Zhang et al., 2011).

In the presence of transfection reagents, AONs are delivered quite efficiently to reaction sites, and consequently, might be placed under single-turnover conditions, while inefficient naked conditions may encourage multiple-turnover conditions. However, it should again be noted that it is difficult to monitor the intracellular turnover reaction in living cells and tissues due to their dynamic nature; thus, further experimental support is necessary to determine whether AONs are actually placed under multiple-turnover conditions at the intracellular antisense reaction site. Nevertheless, our study provides an important opportunity to shed light on the uncertain antisense mechanisms, and may lead to further improvement of the activity and safety profiles of AONs.

Acknowledgments

Author Disclosure Statement

No competing financial interests exist.

References

CROOKE, S.T., LEMONIDIS, K.M., NEILSON, L., GRIFFEY, R., LESNIK, E.A., and MONIA, B.P. (1995). Kinetic characteristics of Escherichia coli RNase H1: cleavage of various antisense oligonucleotide-RNA duplexes. Biochem. J. **312**, 599–608.

CROOKE, T.S. (2007). Antisense Drug Technologies: Principles, Strategies, and Applications. 2nd ed. (CRC Press Taylor & Francis Group, Boca Raton, FL).